microplate. Thereafter, hybridization was detected by staining with the streptavidin-horseradish peroxidase (HRP) conjugate.[15]

Amplifying and sequencing the S region of HBV-DNA

The entire aa sequence of MHR in the S region was amplified by two-stage PCR using genotype-specific primers. The outer primers for the amplification of the first fragment were 5′-TTTCCACCAAGCTCTGCAA-3′ (sense: nt 9–28) and 5′-TTCAGGGAATAACCCCATCT-3′ (antisense: nt 872–853) for genotype A, 5′-CTCCA CCACTTTCCA GACT-3′ (sense: nt 1–22) and 5′-CAACTCCCAATTACATATCCC-3′ (antisense: nt 899–879) for genotype B and 5′-TTACAGGCGGGG TTTTTCTT-3′ (sense: nt 70–89) and 5′-TACAGACTT GGCCCCCAATA-3′ (antisense: nt 771–752) for genotype C. The inner primers were 5′-AGAGTCAGGGGCC TGTATTTT-3′ (sense: nt 35–55) and 5′-AGGGAATAA CCCCATCACTTT-3′ (antisense: nt 869–849) for genotype A, 5′-TTCAAGATCCCAGAGTCAGG-3′ (sense: nt 24–43) and 5′-AGGGAATATCCCCACCTTTTT-3′ (antisense: nt 869–849) for genotype B and 5′-CGGGGTT TTCTTGTTGACA-3′ (sense: nt 77–97) and 5′-CCCAAT ACCACATCATCCATA-3′ (antisense: nt 758–738) for genotype C.

The first stage of amplification was carried out in a thermal cycler for 40 cycles (94°C, 1 min; 55°C, 1 min; 72°C, 1 min) in 100 μL reaction mixture containing 200 mM dNTPs, 1.0 mM each of primers and PCR buffer (50 mM KCl, 10 mM Tris-HCl (pH 8.3), 1.5 mM $MgCl_2$ and 0.001% (wt/vol) gelatin) and 2 U Ampli-Taq polymerase (Perkin Elmer Cetus, Norwalk, CT, USA). PCR products (2 μL) were subjected to the second stage of amplification under the same conditions as those in the first stage. Standard precautions to avoid contamination were taken during PCR, with a negative control serum sample included in each run.

Amplification products were purified on Wizard PCR preps DNA purification resin (Promega, Madison, WI, USA), and sequenced bidirectionally with a Dye Terminator Cycle Sequencing Ready Reaction kit (PE Applied Biosystems, Foster City, CA, USA) using the above-mentioned PCR primers. Sequencing was performed in an automated DNA sequencer (ABI 377; PE Applied Biosystems).

The nucleotide sequences of HBV isolates from the patients were compared with those of three reference HBV strains which are used for vaccine production.[16–18]

Phylogenetic trees were constructed with the Mega Program version 2.1 (Center for Evolutionary Functional Genomics, The Biodesign Institute, Tempe, AZ, USA) using the Kimura two-parameter matrix and the neighbor-joining method.[19] To confirm the reliability of phylogenetic tree analysis, boot-strap resampling, and reconstruction were carried out 500 times.

Hydrophobicity and secondary structure analysis

The hydrophobicity profile of the MHR of the S region was predicted by computer-assisted Kyte-Doolittle analysis (an estimate of hydrophobicity based on the bulk phase partitioning of side chain hydrophobicity alone)[20] with GENETYX-MAC software (version 10.1; Software Development, Tokyo, Japan).

The secondary structures of the amino acids in the same region were predicted by computer-assisted Robson[21] and Chou-Fasman analyses[22] with the GENETYX-MAC software.

Statistical analyses

Data were analyzed by the chi-squared test for categorical data and Student's *t*-test or the Mann–Whitney *U*-test for continuous variables. *P*-values less than 0.05 were regarded as statistically significant.

RESULTS

Distribution and clinical characteristics of HBV genotypes

HEPATITIS B VIRUS genotype was determined in the 48 patients with acute hepatitis B. Genotype A was detected in 11 (23%) patients, genotype B in 11 (23%) and genotype C in 26 (54%).

The clinical and demographic backgrounds of the patients with acute hepatitis B who were infected with HBV of different genotypes are shown in Table 1. The mean ages of all the groups were similar. The proportion of male to female patients was higher in genotype A infection than in genotypes B or C infection (100%, 73% and 64%, respectively: A *vs* B, $P = 0.22$; A *vs* C, $P = 0.01$; B *vs* C, $P = 0.16$). The maximum alanine aminotransferase (ALT) levels were lower in patients with genotype A infection than in patients with genotypes B or C infection (1646 ± 1123, 3085 ± 1119 and 2545 ± 981 IU/L, respectively: A *vs* B, $P = 0.01$; A *vs* C, $P = 0.03$; B *vs* C, $P = 0.89$). The maximum HBV-DNA levels were not significantly different between the

Table 1 Demographic and clinical differences among patients with acute hepatitis infected with HBV of distinct genotypes

Features	Genotypes of HBV			Differences (*P*-value)		
	A ($n=11$)	B ($n=11$)	C ($n=26$)	A *vs* B	A *vs* C	B *vs* C
Age (years)	30.6 ± 7.5	28.1 ± 5.1	31.1 ± 9.1	0.41	0.87	0.33
Gender (M:F)	11:0	8:3	15:11	0.22	0.01	0.16
ALT (IU/L)	1646 ± 1123	3085 ± 1119	2545 ± 981	0.01	0.03	0.89
HBV-DNA (LGE/mL)	6.8 ± 1.7	6.6 ± 2.1	5.2 ± 1.2	0.60	0.23	0.06

ALT, alanine aminotransferase; HBV, hepatitis B virus.

genotypes (6.8 ± 1.7, 6.6 ± 2.1 and 5.2 ± 1.2 LGE/mL, respectively: A *vs* B, $P=0.60$; A *vs* C, $P=0.23$; B *vs* C, $P=0.06$).

Amino acid sequence of the S region

The aa sequence of the S region between aa27 and aa203 was determined in the 48 sequences. Figure 1 shows a phylogenetic tree constructed using the 48 sequences and 15 published sequences (four for genotype A, three for genotype B, three for genotype C, one for genotypes D, E, F, G and H). Among the 48 sequences we studied, 11 were classified into genotype A, 11 into genotype B and 26 into genotype C.

The aa sequence of the region between aa101 and aa163 including MHR (aa111-aa156) was compared among 48 sequences and three HBV sequences (X01587, J02205 and huGK-14) currently used for anti-HBV vaccine production. As shown in Figure 2, the aa sequences of X01587 (used for Bimmugen) and J02205 (used for Heptavax) differed in eight amino acids (i.e. aa110, aa113, aa114, aa126, aa131, aa143, aa160 and aa161). The aa sequence of huGK-14, which is used for the HBV-vaccine Meinyu, differed from that of X01587 in six amino acids and from that of J02205 in two amino acids.

Nine of the 11 isolates classified into genotype A had the same aa sequence as J02205. The remaining two isolates (AB289727 and AB289728) differed from J02205 at aa161 (Fig. 2).

Ten of the 11 isolates classified into genotype B had the same aa sequence as J02205 except for two amino acids (aa114 and aa131). The remaining isolate had another aa substitution at aa112 (Fig. 2).

As shown in Figure 2, 22 of the 26 isolates classified into genotype C had the same sequence as X01587. The remaining four isolates (from patients 10, 24, 30 and 48) had the same sequence as X01587 except for one aa substitution at aa131; the threonine (aa131) of X01587 was substituted with proline for three isolates (AB289714, AB289720 and AB289736) and with alanine for one isolate (AB289701).

Hydrophobicity and secondary structure analysis

As mentioned above, the aa sequences of the MHR from four isolates differed from that of X01587 only at aa131. Furthermore, the aa sequence of the MHR differed between X01587 and J2205 in eight amino acids. We compared the hydropathy and secondary structure of the MHR among J02205, X01587 and two isolates with genotype C (one isolate with proline at aa131 and one with alanine at aa131). The results of Kyte-Doolittle hydropathy analysis based on the hydropathy index are shown in Figure 3. The substitution with alanine-131 was found to alter the patterns on the hydropathy plot, whereas the substitution with proline-131 was found to have little effect. A substitution with alanine-131 could increase the hydrophobicity of the first loop of the MHR, which may affect the antigenicity of HBV.

The secondary structure of our isolate with alanine-131 by Chou-Fasman analysis predicted an α-helix configuration for the region from aa126 to aa135 instead of the β-configuration predicted for the same region of X01587. The predicted secondary structure of our isolate with proline-131 coincided with that of X01587. In contrast, by Robson prediction, the secondary structure of our isolate with alanine-131 coincided with that of X01587; however, that of our isolate with proline-131 was found to have lost a turn structure between aa131 and aa134, which was predicted for X01587.

DISCUSSION

VACCINATION IS THE key to controlling HBV infection. In countries with a high prevalence of HBV infection, universal vaccination is effective not only for controlling viral infections but also for decreasing the incidence of hepatocellular carcinoma.[5,23] Even in

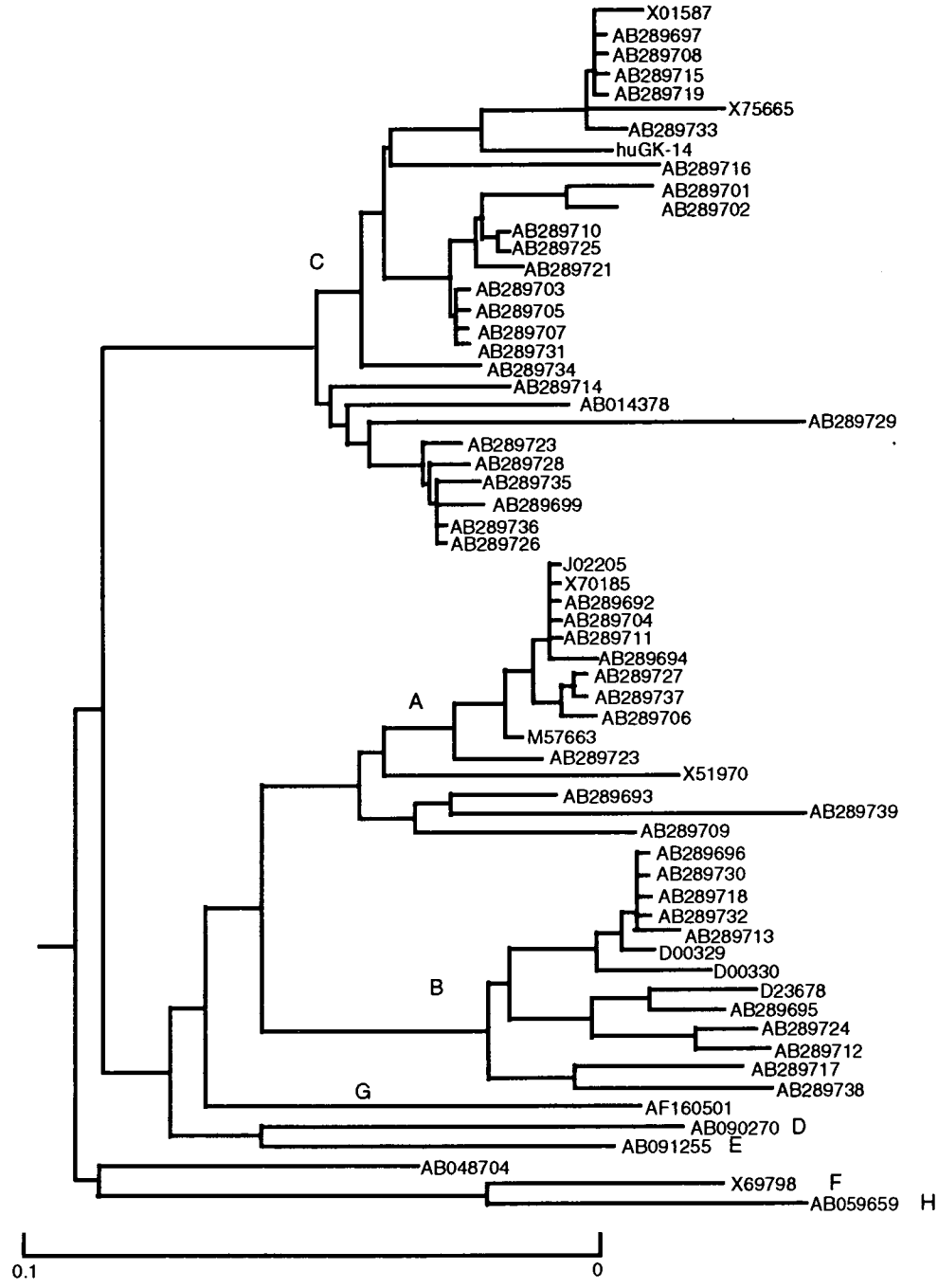

Figure 1 Phylogenetic tree constructed using hepatitis B virus (HBV)-DNA sequences of the *S* gene. The sequences include four with genotype A, four with genotype B, three with genotype C, and those recovered from the serum of 48 patients with acute hepatitis B. J02205 (genotype A) is used for the production of Heptavax and X01587 (genotype C) is used for the production of Bimmugen. The horizontal bar indicates the number of nucleotide substitutions per site. Accession numbers are shown for the isolates that have been deposited in the DDBJ/EMBL/GenBank databases. The accession numbers for the HBV sequences from the 48 patients are also shown.

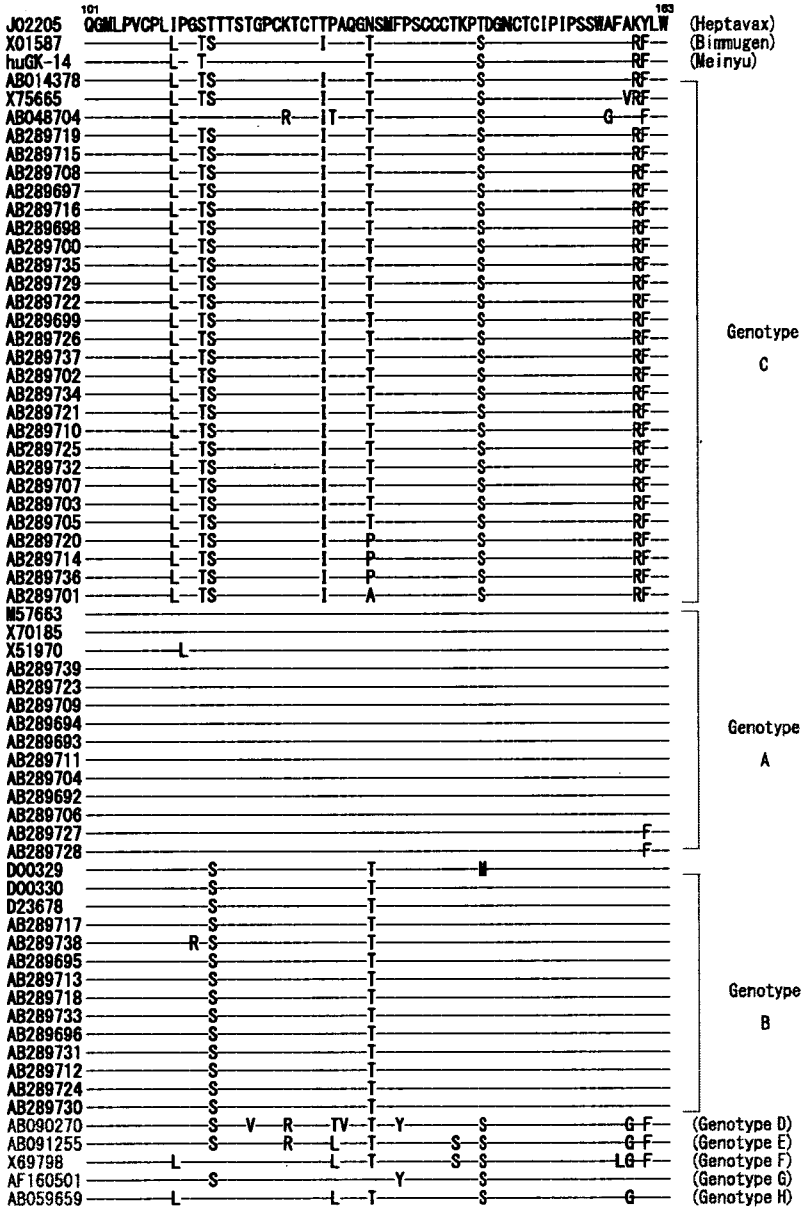

Figure 2 Comparison of amino acid sequences of the major hydrophilic region (MHR) of the *S* gene.

countries with a low prevalence of HBV infection, vaccination is very important for preventing mother-to-child transmission as well as patient-to-staff transmission.

HBV is classified into several genotypes that differ from one another in nucleotide sequence by more than 8% of the entire genome. The aa sequences of their phenotypes also differ among genotypes. The difference in the aa sequence of the 'a' determinant region may alter the three-dimensional structure and antigenicity, and may reduce the protectivity of HBV vaccines.

As mentioned above, the aa sequences of currently available recombinant vaccines differ from each other. J02205 and X01578 differ in eight amino acids (i.e. aa110, aa113, aa114, aa126, aa131, aa143, aa160 and aa161) between aa101 and aa163. Three (i.e. aa126, aa131 and aa143) of them are included in the MHR and may alter the hydropathy and three-dimensional

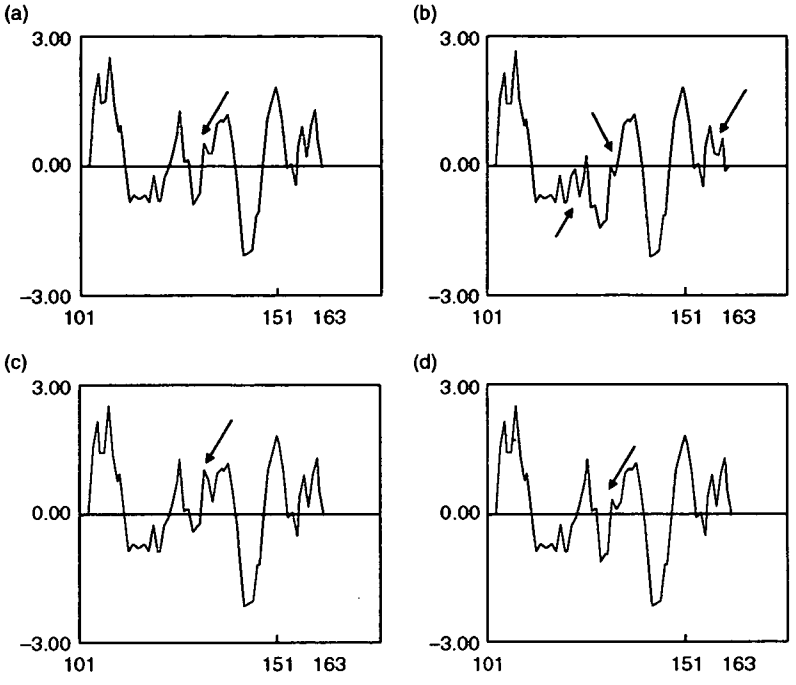

Figure 3 Hydropathy profile of the major hydrophilic region (MHR) of the *S* gene elaborated using the Kyte-Doolittle hydropathy index. Arrows show the positions of amino acids which are different among X01587, J02205, AB289701 (alanine-131) and AB289720 (proline-131). (a) X01587, (b) J02205, (c) AB289701 (alanine-131), (d) AB289720 (proline-131).

structure of the region. Therefore, the antibody produced against J02205 vaccines may not completely neutralize X01578 and vice versa. Indeed, previous studies showed that antibody profiles induced by recombinant vaccines produced from different genotypes are not identical with each other,[12] which suggests that antibodies produced by recombinant vaccines might not protect viral infection with different genotypes.

As shown in Figure 2, the aa sequences of our isolates classified into genotype A are very close to the aa sequence of J02205. Therefore, the transmission of genotype A HBV is prevented by Heptavax which is made from J02205.

The aa sequences of our isolates classified into genotype B are the same as the aa sequence of J02205 except for one substitution at aa131. This aa, which is asparagine and is located in the first stem loop structure of the MHR, was substituted with threonine in our genotype B isolates. Because asparagine and threonine have an uncharged side chain and similar polarity, genotype B HBV infection may be prevented effectively by Heptavax.

The aa sequences of our isolates classified into genotype C were the same as that of X01587 except for four isolates having a substitution at aa131. Bimmugen, which is produced from X01587, may be effective for preventing genotype C HBV infections caused by those four isolates. However, Heptavax may not be effective for preventing genotype C HBV infection because of the difference in eight amino acids as described above.

The four isolates have proline or alanine instead of threonine-131, which has never been reported before. The polarities of threonine and proline/alanine are quite different. The Kyte-Doolittle hydropathy analysis suggests that substituting threonine at aa131 with alanine or proline would increase hydrophobicity, which may then lead to a change in antigenicity. Hou *et al.* reported that some blood donors who were tested negative for serum HBsAg had a substitution of isoleucine for threonine at aa131 in the S region.[24] They suggested that the structure and antigenicity of HBV may be altered by this substitution.

The secondary structure of our isolate with alanine-131 predicted by Chou-Fasman analysis suggested an α-helix configuration instead of a β-configuration in the region from aa126 to aa135. The secondary structure of our isolate with proline-131 predicted by Robson analysis suggested that this change causes the loss of a turn structure between aa131 and aa134. Some changes in the secondary structure can affect the three-dimensional structure of the protein and thus affect antigenicity. These results suggest that the transmission of the four

isolates with an aa substitution at aa131 may not be prevented by either Heptavax or Bimmugen.

However, the protective immunity elicited by HBV vaccines, which is usually polyclonal in nature, may not be totally lost or severely affected *in vivo* by the alteration of only a single amino acid in the 'a' determinant region.[25] Also, antibodies against regions outside the 'a' determinant region may be protective.[26] The protectivity of current vaccines may be elucidated by *in vitro* binding studies using polyclonal antibodies.

It was reported that some individuals immunized with recombinant vaccines are infected with HBV with or without mutations in the 'a' determinant region.[11,27,28] HBV isolates with amino acid substitutions at aa144[29–31] or 145[11,27,28] are known to be transmitted despite vaccination. Indeed, some chronic HBV carriers are reported to have HBV with such amino acid substitutions.[32,33] We were unable to find patients who had these substitutions in the present study. However, large-scale studies are necessary to elucidate the prevalence of 'vaccine-escape mutants' in patients with acute hepatitis B.

In conclusion, we have shown that the aa sequence of the MHR in the *S* gene of HBV is different among isolates from patients with acute HBV infection. Current vaccination may prevent the transmission of these HBV isolates, which should be further investigated.

ACKNOWLEDGMENT

WE THANK MS Yoriko Kajiki for her excellent technical assistance. We are grateful to doctors Kozo Ishidate and Yoshimasa Machida for helpful discussions. This work was supported in part by Health Sciences Research Grants from the Ministry of Health, Labor, and Welfare of Japan.

REFERENCES

1 Manno M, Camma C, Schepis F *et al.* Natural history of chronic HBV carriers in northern Italy: morbidity and mortality after 30 years. *Gastroenterology* 2004; **127**: 756–63.
2 Liaw YF, Lin DY, Chen TJ, Chu CM. Natural course after the development of cirrhosis in patients with chronic type B hepatitis: a prospective study. *Liver* 1989; 9: 235–41.
3 Fattovich G, Brollo L, Giustina G *et al.* Natural history and prognostic factors for chronic hepatitis type B. *Gut* 1991; 32: 294–8.
4 Liaw YF, Tai DI, Chu CM, Chen TJ. The development of cirrhosis in patients with chronic type B hepatitis: a prospective study. *Hepatology* 1988; 8: 493–6.
5 Chang MH, Chen CJ, Lai MS *et al.* Universal hepatitis B vaccination in Taiwan and the incidence of hepatocellular carcinoma in children. Taiwan Childhood Hepatoma Study Group. *N Engl J Med* 1997; 336: 1855–9.
6 Ni YH, Chang MH, Huang LM *et al.* Hepatitis B virus infection in children and adolescents in a hyperendemic area: 15 years after mass hepatitis B vaccination. *Ann Intern Med* 2001; 135: 796–800.
7 Tanaka J, Kumagai J, Katayama K *et al.* Sex- and age-specific carriers of hepatitis B and C viruses in Japan estimated by the prevalence in the 3 485 648 first-time blood donors during 1995–2000. *Intervirology* 2004; 47: 32–40.
8 Kobayashi M, Suzuki F, Arase Y *et al.* Infection with hepatitis B virus genotype A in Tokyo, Japan during 1976 through 2001. *J Gastroenterol* 2004; 39: 844–50.
9 Yotsuyanagi H, Okuse C, Yasuda K *et al.* Distinct geographic distributions of hepatitis B virus genotypes in patients with acute infection in Japan. *J Med Virol* 2005; 77: 39–46.
10 Suzuki Y, Kobayashi M, Ikeda K *et al.* Persistence of acute infection with hepatitis B virus genotype A and treatment in Japan. *J Med Virol* 2005; 76: 33–9.
11 Water JA, Kennedy M, Voet P *et al.* Loss of the common 'A' determinant of hepatitis B surface antigen by a vaccine-induced escape mutant. *J Clin Invest* 1992; 90: 2543–7.
12 Heijtink RA, Schneeberger PM, Postma B, Crombach W. Anti-HBs levels after hepatitis B immunisation depend on test reagents: routinely determined 10 and 100 IU/L seroprotection levels unreliable. *Vaccine* 2002; 20: 2899–905.
13 Hieu NT, Kim KH, Janowicz Z, Timmermans I. Comparative efficacy, safety and immunogenicity of Hepavax-Gene and Engerix-B, recombinant hepatitis B vaccines, in infants born to HBsAg and HBeAg positive mothers in Vietnam: an assessment at 2 years. *Vaccine* 2002; 20: 1803–8.
14 Kamisango K, Kamogawa C, Sumi M *et al.* Quantitative detection of hepatitis B virus by transcription-mediated amplification and hybridization protection assay. *J Clin Microbiol* 1999; 37: 310–14.
15 Kato H, Orito E, Sugauchi F *et al.* Frequent coinfection with hepatitis B virus strains of distinct genotypes detected by hybridization with type-specific probes immobilized on a solid-phase support. *J Virol Methods* 2003; 110: 29–35.
16 Koike K, Yoshida E, Katagiri K *et al.* Production of hepatitis B virus surface antigen particles by the human hepatoma cell line huGK-14 in a serum-free medium. *Jpn J Cancer Res* 1987; 78: 1341–6.
17 McAleer WJ, Buynak EB, Maigetter RZ, Wampler DE, Miller WJ, Hilleman MR. Human hepatitis B vaccine from recombinant yeast. *Nature* 1984; 307: 178–80.
18 Valenzuela P, Medina A, Rutter WJ, Ammerer G, Hall BD. Synthesis and assembly of hepatitis B virus surface antigen particles in yeast. *Nature* 1982; 298: 347–50.
19 Sugita S, Yoshioka Y, Itamura S *et al.* Molecular evolution of hemagglutinin genes of H1N1 swine and human influenza A viruses. *J Mol Evol* 1991; 32: 16–23.

20 Kyte J, Doolittle F. A simple method for displaying the hydropathic character of a protein. *J Mol Biol* 1982; 157: 105–32.
21 Garnier J, Osguthorpe DJ, Robson B. Analysis of the accuracy and implications of simple methods for predicting the secondary structure of globular proteins. *J Mol Biol* 1978; 120: 97–120.
22 Chou PY, Fasman GD. Conformational parameters for amino acids in helical, β-sheet, and random coil regions calculated from proteins. *Biochemistry* 1974; 13: 211–12.
23 Ni YH, Chang MH, Huang LM *et al.* Hepatitis B virus infection in children and adolescents in a hyperendemic area: 15 years after mass hepatitis B vaccination. *Ann Intern Med* 2001; 135: 796–80.
24 Hou J, Wang Z, Cheng J *et al.* Prevalence of naturally occurring surface gene variants of hepatitis B virus in nonimmunized surface antigen-negative Chinese carriers. *Hepatology* 2001; 34: 1027–34.
25 Ogata N, Cote PJ, Zanetti AR *et al.* Licensed recombinant hepatitis B vaccines protect chimpanzees against infection with the prototype surface gene mutant of hepatitis B virus. *Hepatology* 1999; 30: 779–86.
26 Paulij WP, de Wit PL, Sunnen CM *et al.* Localization of a unique hepatitis B virus epitope sheds new light on the structure of hepatitis B virus surface antigen. *J Gen Virol* 1999; 80: 2121–6.
27 Carman WF, Zanetti AR, Karayiannis P *et al.* Vaccine-induced escape mutant of hepatitis B virus. *Lancet* 1990; 336: 325–9.
28 Carman WF, Korula J, Wallace L, MacPhee R, Mimms L, Decker R. Fulminant reactivation of hepatitis B due to envelope protein mutant that escaped detection by monoclonal HBsAg ELISA. *Lancet* 1995; 345: 1406–7.
29 Lee PI, Chang LY, Lee CY, Huang LM, Chang MH. Detection of hepatitis B surface gene mutation in carrier children with or without immunoprophylaxis at birth. *J Infect Dis* 1997; 176: 427–30.
30 Protzer-Knolle U, Naumann U, Bartenschlager R *et al.* Hepatitis B virus with antigenically altered hepatitis B surface antigen is selected by high-dose hepatitis B immune globulin after liver transplantation. *Hepatology* 1998; 27: 254–63.
31 Shields PL, Owsianka A, Carman WF *et al.* Selection of hepatitis B surface 'escape' mutants during passive immune prophylaxis following liver transplantation: potential impact of genetic changes on polymerase protein function. *Gut* 1999; 45: 306–9.
32 Yamamoto K, Horikita M, Tsuda F *et al.* Naturally occurring escape mutants of hepatitis B virus with various mutations in the S gene in carriers seropositive for antibody to hepatitis B surface antigen. *J Virol* 1994; 68: 2671–6.
33 Kato J, Hasegawa K, Torii N, Yamauchi K, Hayashi N. A molecular analysis of viral persistence in surface antigen-negative chronic hepatitis B. *Hepatology* 1996; 23: 389–95.

research articles Journal of proteome research

A Proteomics Method Revealing Disease-Related Proteins in Livers of Hepatitis-Infected Mouse Model

Tomoko Ichibangase,[†] Kyoji Moriya,[‡] Kazuhiko Koike,[‡] and Kazuhiro Imai*[,†]

Research Institute of Pharmaceutical Sciences, Musashino University, 1-1-20 Shinmachi, Nishitokyo-shi Tokyo, Japan 202-8585, and Department of Internal Medicine, Graduate School of Medicine, University of Tokyo, 7-3-1 Hongo, Bunkyo-ku, Tokyo, Japan 113-8655

Received February 19, 2007

In this post-genome era, a sensitive quantitative method is required for differential profiling analyses of clinical proteomes to understand the disease progress. Here, we adopt the FD-LC–MS/MS method, consisting of fluorogenic derivatization (FD), separation by liquid chromatography (LC), and identification by LC-tandem mass spectrometry (MS/MS), to reveal disease-related proteins in livers of hepatocarcinogenesis in transgenic (Tg) and non-transgenic (NTg) mice at three developmental stages. After 6 months, the expression of apoptosis-related proteins is suppressed. After 12 months, proteins related to respiration, the electron-transfer system, and anti-oxidation are significantly up-regulated. After 16 months, proteins related to defense, β-oxidation, and apoptosis are significantly suppressed. This fluctuating expression of proteins could explain the progression of hepatocarcinogenesis. The method would be useful for clinical proteomics analysis because of its high resolution, sensitivity, and reproducibility.

Keywords: DAABD-Cl • FD-LC–MS/MS method • core protein • hepatitis C • liver protein • fluorogenic derivatization

Introduction

Recent work in clinical proteomics has involved quantitative and comparative studies of mixture composition and/or the relative abundance of proteins under differing physiologically relevant conditions and differing experimental approaches, commonly referred to as differential profiling. Numerous approaches have been employed for protein quantification, including a one- or two-dimensional gel electrophoretic and liquid chromatographic (LC) method, followed by mass spectrometry (MS).[1–4] Each of the technical approaches has advantages and limitations. For example, gel-based methods are based on the densitometric quantification of proteins visualized using dyes on gel, followed by in-gel enzymatic digestion of the subject protein spots, with the resulting peptides then subjected to MS analysis. This approach has been widely practiced in proteomics studies because of its high resolution, which enables separating the protein isoforms and post-translational modifications. However, this method suffers from a lack of reproducibility, low sensitivity, low dynamic range, and difficulty in resolving proteins with extreme hydrophobicity or isoelectric points, among other issues.[2,3,5,6] In recent years, the introduction of differential gel electrophoresis (DIGE) using fluorescence reagents such as CyDye DIGE Fluor minimal dye[6–8] and saturation dye[9,10] has somewhat improved the reproducibility, sensitivity, and dynamic range.

LC-based methods offer flexibility of choice over a wide range of stationary and mobile phases to resolve complex biological samples at the protein or peptide level. In these methods, proteins are usually digested into peptides prior to separation by separation columns. The advantage of this approach is that the resolved peptides from the column can be directly introduced into an MS system. To obtain high sensitivity and quantification, the stable-isotope labeling reagents, that is, the isotope-coded affinity tag (ICAT),[11] the cleavable ICAT (cICAT),[3,12,13] and isobaric tags for relative and absolute quantitation (iTRAQ),[3,14] were developed and have gained in popularity. However, a major disadvantage of these strategies is that the obtained peptides cannot be correctly identified as any given protein. Moreover, low-abundance peptides are masked by high-abundance peptides with similar m/z ratios. Thus, for highly complex samples, such as tissue homogenates, these methods are not suitable for the quantification of specific low-abundance proteins unless extensive purification is employed before analysis.[2–4,12,13]

We recently reported a method for proteomics studies called the FD-LC–MS/MS method.[15–18] This method involves fluorogenic derivatization (FD) of proteins using fluorogenic reagents such as 7-chloro-*N*-[2-(dimethylamino)ethyl]-2,1,3-benzoxadiazole-4-sulfonamide (DAABD-Cl), followed by HPLC separation of the derivatized proteins, isolation of the subject proteins, enzymatic digestion of the isolated proteins, and identification of the proteins utilizing HPLC and tandem MS with a database-searching algorithm. The FD-LC–MS/MS method has unique features, differing from other proteome approaches in using a fluorogenic reagent to derivatize proteins

* To whom correspondence should be addressed at 1-1-20 Shinmachi, Nishitokyo-shi Tokyo 202-8585, Japan. Tel. +81-42-468-9787. Fax +81-42-468-9787. E-mail: k-imai@musashino-u.ac.jp.
† Musashino University.
‡ University of Tokyo.

10.1021/pr070094c CCC: $37.00

Published on Web 06/09/2007

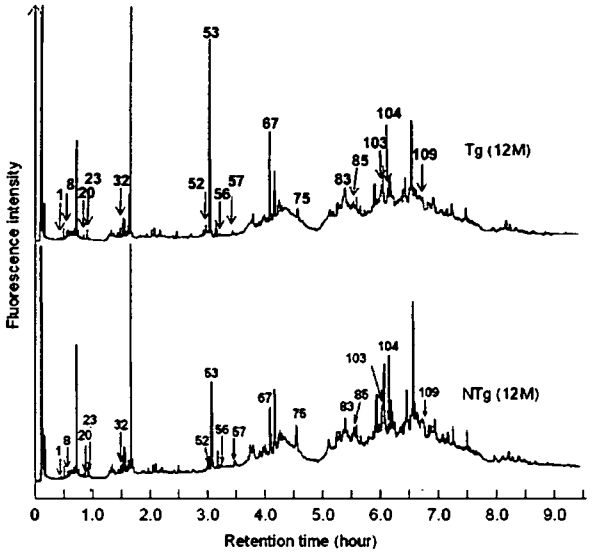

Figure 1. Chromatograms of proteins (8.0 μg protein) in mouse liver derivatized with DAABD-Cl. The chromatograms above and below were obtained from transgenic (12 months) and non-transgenic (12 months) mice, respectively. The altered peaks (106 proteins) between transgenic and non-transgenic mice were numbered, and as representatives, significantly altered peaks (15 proteins) and a peak (no. 53 for accuracy measurement) are described.

and HPLC to separate the derivatized proteins. The fluorogenic reagent is highly reactive and selective to thiols, is nonfluorescent itself, and is water-soluble, so there are few limitations to the complete derivatization of cysteine residues of proteins. The proposed method enables highly sensitive detection of derivatized proteins at the femtomol level,[17,18] whereas other derivatized reagents, such as CyDye DIGE Fluoro minimal dye, would have difficulty forcing the labeling reaction into saturation.[7,8] Separation by HPLC led to highly reproducible quantification. In addition, a protein can be isolated and identified from the corresponding peak fraction without losing any amino acid sequence information, including protein isoforms and post-translational modifications, because the isolated protein itself is digested into peptides following isolation by HPLC. Although this method has already identified more than 100 proteins in a soluble extract of *Caenorhabditis elegans*[15-17] and has identified altered proteins in the islet of Langerhans in dexamethazone-treated rats,[18] there have been no studies involving clinical proteomics analysis utilizing DAABD-Cl as a fluorogenic reagent. Therefore, we attempted to apply it to the quantification and differential profiling analysis of liver proteins taken from hepatitis C virus (HCV) core gene transgenic (Tg) and non-transgenic (NTg) as a model. HCV is the main cause of chronic hepatitis. Chronic hepatitis ultimately results in the progression of hepatocellular carcinoma (HCC). However, the mechanism of hepatocarcinogenesis associated with HCV infection is still unclear. K. Moriya et al. have suggested that the HCV core protein plays a critical role in the progression of HCC and that transgenic mice provide a good animal model for determining the molecular and pathological events in hepatocarcinogenesis with HCV infection.[19-22] Such mice have been investigated previously in terms of morphological and biochemical changes in HCV infection, so far. Therefore, this study investigated the long-term consequences of HCV core gene expression from the viewpoint of proteomics and evaluated the proposed method as the quantification and differential profiling analysis.

Materials and Methods

Transgenic Mice. The production of HCV core gene transgenic mice has been described.[19] Because HCC develops preferentially in male transgenic mice, male mice were used for analysis. Male non-transgenic littermates were utilized as controls. At least three mice were used in each experiment, with the data then subjected to statistical analysis. In the previous studies,[19,20] these transgenic mice developed hepatic steatosis, one of the characteristic histological features of chronic hepatic C, as early as 3 months of age. As the mice grew to 12 months of age, steatosis slowly progressed without neoplastic change. At the age of 16 months, one-fourth of the male mice had experienced hepatic tumors. Moreover, older transgenic mice (>12 months of age) morphologically exhibited an age-dependent increase in oxidative stress. Therefore, in this study, the transgenic and non-transgenic mice used were aged 6, 12, and 16 months, representing the early, medium, and late stages of hepatocarcinogenesis. Also, to exclude the influence of protein variations with advancing age, the amount of protein change due to HCV infection was calculated based on the Tg-to-NTg (Tg/NTg) ratio. All studies were performed according to the Helsinki Declaration and have passed our institutional review board.

Preparation of Sample and Determination of Total Proteins. Liver samples (100 mg) were homogenized in 500 μL of 10 mM CHAPS aq with a pestle on ice. The homogenate was centrifuged at 20 400g for 15 min at 4 °C. The supernatant was then collected and stored as a soluble fraction at −20 °C until use. The liver total proteins were determined with the Quick Start Bradford Protein assay kit (Bio-Rad Laboratories, Inc.) by following the written instructions. Bovine serum albumin was used as a protein standard.

FD and HPLC Conditions. The previous method[16] was used for the FD procedure for liver proteins with DAABD-Cl, except that the borate buffer was replaced with a pH 8.7 buffer solution (6.0 M guanidine hydrochloride, Tokyo Chemical Industry). Briefly, homogenized liver tissue was diluted with the CHAPS aq to 4.0 mg/mL, and 10 μL of the sample was mixed with 60 μL of a mixture of 0.83 mM Tris (2-carboxyethyl) phosphine hydrochloride (TCEP), ethylenediamine-*N,N,N',N'*-tetraacetic acid sodium salt (Na_2EDTA), and 16.6 mM CHAPS in the pH 8.7 buffer solution; 25 μL of the buffer solution; and 5.0 μL of 140 mM DAABD-Cl in acetonitrile. After the reaction mixture was placed in a 40 °C water bath for 10 min, 3.0 μL of 20% trifluoroacetic acid (TFA) was added to stop the derivatization reaction. Twenty microliters of the reaction mixture (8.0 μg proteins) was injected into the HPLC system at a flow rate of 0.55 mL/min. The overall system consisted of a Hitachi L-7000 series HPLC system and a fluorescence detector (Jasco FP-2025 plus; λex. 395 nm; λem, 505 nm). Since the derivatives offer adaptable selectivity for the stationary phase, a protein column (Intrada WP-RP, 250 × 4.6 mm i.d., Imtakt Co.) with a column temperature of 60 °C was adopted to further improve the column separation. The mobile phases consisted of 0.15% TFA in acetonitrile/isopropanol/water (A) 9.0/1.0/90 and (B) 69/1.0/30. Mobile phase (C) was the same as (A), except with 0.20% TFA. The gradient condition was established with the following elution: 5.0% B and 1.0% C held for 5.0 min; to 30% B and 35% C in 30 min, and then held for 35 min; to 35% B and 35%

Table 1. Altered Proteins between Tg and NTg Mouse Livers for 6 Months[a]

peak number	Tg/NTg ratio	protein name	molecular mass (Da)	GI number[b]
		Down-Regulated		
		marker		
54	0.55	Major urinary protein (MUP)	20680	gi|295910
56	0.64*	MUP	17549	gi|53271
58	0.58	MUP	17549	gi|53271
55	0.63	Glial fibrillary acidic protein	46498	gi|14193690
		respiration		
52	0.52*	α-globin	15076	gi|49901
		electron-transfer system		
57	0.64	ATP synthase, H+ transporting, mitochondrial F0 complex, subunit d	18752	gi|16741459
		apoptosis		
1	0.54*	Eukaryotic translation elongation factor 1 α 1 (EF-1 α 1)	50140	gi|13278382
		glycolytic system		
77	0.74	PREDICTED: similar to Glyceraldehyde-3-phosphate dehydrogenase (GAPDH)	35789	gi|51768209
		other		
34	0.62	ND***		
		Up-Regulated		
		respiration		
27	1.28	α-globin	15076	gi|49900
29	1.28	α-globin	15076	gi|49900
37	1.35	α-globin	15076	gi|49900
		defense		
44	1.14	Cu/Zn-superoxide dismutase (SOD)	15955	gi|201006
75	1.69	Glycine *N*-methyltransferase	32712	gi|15679953
78	1.22	Aldo-keto reductase family 1, member C6	37024	gi|13487925
79	1.32	Glutathione S-transferase, mu 1	25953	gi|61402231
95	1.29	Glutathione S-transferase, α 3	25344	gi|31981724
		fatty acid metabolism (containing *β*-oxidation)		
35	1.43	Fatty acid-binding protein, hepatic (fragment)	10173	gi|90485
36	1.24	Fatty acid-binding protein, hepatic (fragment)	10173	gi|90485
42	1.37	Fatty acid-binding protein, hepatic (fragment)	10173	gi|90485
82	1.31	Acetyl-Coenzyme A acyltransferase 2 (mitochondrial 3-oxoacyl-Coenzyme A thiolase)	41831	gi|20810027
		apoptosis		
3	2.21	EF-1α1	50140	gi|13278382
		glycolytic system		
61	1.40	Fructose-bisphosphate aldolase B	39548	gi|15723269
99	1.36	Enolase 1, α non-neuron	47095	gi|12963491
		metabolism		
68	1.37	Carbonic anhydrase 3	29348	gi|31982861
		other		
26	1.41	Unnamed protein product	58587	gi|12852157
33	1.40	Unnamed protein product	57807, 58587, 57007, 52653	gi|12852157, gi|26345440, gi|2634914, gi|26349459
112	1.42	put. *β*-Actin (aa 27–375)	39161	gi|49868

[a] Peak numbers correspond to those in Figure 1. Asterisks indicate significant differences (two-tailed Student's *t* test, *$P \leq 0.05$, ** $P \leq 0.01$). ***ND, not detected. [b] GI number is simply a series of digits that are assigned consecutively to each sequence record processed by NCBI. The GI system of sequence identifiers runs parallel to the accession.version system, which was implemented by GenBank, EMBL, and DDBJ in February 1999. Therefore, if the protein sequence changes in any way, it will receive a new GI number. (http://www.ncbi.nlm.nih.gov/Sitemap/samplerecord.html#ProteinIDB).

C in 70 min, then to 38% B and 35% C in 130 min; to 44% B and 55% C in 250 min, and then held for 50 min; to 47% B and 53% C in 330 min; to 60% B and 40% C in 480 min; to 70% B and 30% C in 520 min; and then to 90% B and 10% C in 570 min.

Because of the differential profiling of proteins in transgenic and non-transgenic mice, the corresponding peak heights in the different elution profiles were compared for each month age. The correspondence of the peak was judged not only from the specific retention time of the derivatives, but also confirmation of the protein following isolation and identification of the derivatives. The Tg/NTg ratio was also compared between three developmental stages to investigate the consequences of HCV core gene expression during the progression of hepatocarcinogenesis.

Identification of Derivatized Proteins. Each eluate of the subject proteins was concentrated to 5.0 μL under reduced pressure. The residue was diluted with 50 μL of 50 mM ammonium bicarbonate solution (pH 7.8) containing 0.50 U trypsin and 10 mM calcium chloride, and the resultant mixture was incubated for 2.0 h at 37 °C. The peptide mixture (20 μL) was directly subjected to a nanoLC–ESI-tandem MS spectrometer (HCT plus, Bruker Daltonics). Chromatography was performed using an Ultimate/Famos/Switchos suite of instruments (LC Packings, Dionex). The sample was loaded onto a nanoprecolumn (300 μm i.d. × 1.0 mm, C18 PepMap) in the

Table 2. Altered Proteins between Tg and NTg Mouse Livers for 12 Months[a]

peak number	Tg/NTg ratio	protein name	molecular mass (Da)	GI number[b]
		Down-Regulated		
		respiration		
29	0.64	α-globin	15076	gi|49900
		defense		
75	0.56	Glycine *N*-methyltransferase	32712	gi|15679953
76	0.72	Glutathione *S*-transferase, mu 1	25953	gi|61402231
91	0.79	Methionine adenosyltransferase I, α	43481	gi|19526790
		fatty acid metabolism (containing β-oxidation)		
36	0.74	Fatty acid-binding protein, hepatic	10173	gi|90485
40	0.80	Fatty acid-binding protein, hepatic	10173	gi|90485
102	0.77	Peroxisomal acyl-CoA oxidase	74608	gi|2253380
		metabolism		
68	0.75	Carbonic anhydrase 3	29348	gi|31982861
105	0.80	Aldehyde dehydrogenase family 1, subfamily A1	54447	gi|7304881
		amino acid synthesis		
80	0.61	4-Hydroxyphenylpyruvate dioxygenase	45054	gi|849053
		other		
106	0.68	Heat-responsive protein	18462	gi|1255116
		Up-Regulated		
		marker		
55	1.52	Glial fibrillary acidic protein	46498	gi|14193690
56	1.23	MUP	17549	gi|53271
58	1.68	MUP	17549	gi|53271
70	1.51	α-Fetoprotein	47195	gi|191765
		respiration		
4	2.50	Hemoglobin, β adult major chain	15738	gi|31982300
66	1.45	Hemoglobin, β adult major chain	15738	gi|31982300
67	1.98*	Hemoglobin β	15653	gi|229301
27	2.27	α-globin	15076	gi|49900
28	2.43	α-globin	15076	gi|49900
30	1.70	α-globin	15076	gi|49901
31	1.64	α-globin	15076	gi|49900
51	2.12	α-globin	15076	gi|49900
53	2.05	α-globin	15076	gi|49902
		electron-transfer system		
20	1.85*	ATP synthase, H+ transporting, mitochondrial F1 complex, epsilon subunit	5834	gi|13385484
57	1.56*	ATP synthase, H+ transporting, mitochondrial F0 complex, subunit d	18752	gi|16741459
		protein synthesis		
10	2.43	Ribosomal protein L28	15700	gi|56541228
46	2.33	Ribosomal protein S16	16319	gi|70920
		defense		
9	1.80	SOD	15955	gi|201006
11	2.28	SOD	15752	gi|226471
15	1.24	SOD	15955	gi|201006
18	1.96	SOD	15955	gi|201006
44	1.85	SOD	15955	gi|201006
12	1.42	60S Ribosomal protein	24692	gi|899445
43	1.31	Thioredoxin 1	11668	gi|6755911
50	1.99	Chain C, Crystal Structure Of Macrophage Migration Inhibitory Factor	12365	gi|5542287
69	1.60	D-Dopachrome tautomerase	13069	gi|6753618
71	2.24	Albumin 1	68648	gi|19353306
73	2.11	Albumin 1	68648	gi|19353306
89	1.63	Albumin 1	68648	gi|19353306
83	1.47**	Betaine-homocysteine methyltransferase (BHMT)	44992	gi|62533211
90	2.17	Methionine adenosyltransferase I, α	43481	gi|19526790
100	1.25	Glycine *N*-methyltransferase	32712	gi|15679953
		fatty acid metabolism (containing β-oxidation)		
7	1.95	3-Ketoacyl-CoA thiolase B	43968	gi|18043769
35	1.27	Fatty acid-binding protein, hepatic - (fragment)	10173	gi|90485
41	1.28	Fatty acid-binding protein, hepatic - (fragment)	10173	gi|90485
82	1.32	Acetyl-Coenzyme A acyltransferase 2 (mitochondrial 3-oxoacyl-Coenzyme A thiolase)	41831	gi|20810027
		apoptosis		
1	2.86	EF-1α1	50139	gi|13278381
2	2.79	EF-1α1	50140	gi|13278382
3	1.64	EF-1α1	50140	gi|13278382
8	2.02	Ribosomal protein S29, isoform 1	6672	gi|22267962
24	2.06	Ribosomal protein L14	23549	gi|13385472

Table 2. (Continued)

peak number	Tg/NTg ratio	protein name	molecular mass (Da)	GI number[b]
		glycolytic system		
59	2.96	Fructose-bisphosphate aldolase B	39548	gi|15723268
62	1.21	Fructose-bisphosphate aldolase B	39548	gi|15723268
77	1.39	PREDICTED: similar to GAPDH	35789	gi|51768209
112	1.64	Lactate dehydrogenase 1, A chain	36475	gi|6754524
		metabolism		
21	1.79	TI-225	14167	gi|1167510
22	2.02	TI-225	14167	gi|1167510
32	2.02	Cystatin B	11039	gi|6681071
72	3.23	Carbonic anhydrase 3	29348	gi|31982861
104	1.83*	Acetaldehyde dehydrogenase (ALDH)	54410	gi|9755362
110	1.82	Aldh2 protein	56502	gi|13529509
115	1.90	Malate dehydrogenase (EC 1.1.1.37)	31692	gi|164543
116	2.10	Argininosuccinate lyase	51707	gi|19526986
		signal transduction		
47	1.70	Phosphatidylethanolamine binding protein	20847	gi|9256572
		amino acid synthesis		
74	2.21	Glycine-*N*-acyltransferase	34076	gi|22122359
		other		
5	2.02	ND***		
6	1.99	ND***		
118	1.97	ND***		
19	3.56	γ-actin	40992	gi|809561
23	1.40*	Diazepam binding inhibitor, splice form 1b	15219	gi|67511482
39	2.80	Saposin	61353	gi|249387
45	2.13	Unnamed protein product	58587, 57007, 52653, 49471	gi|12852157, gi|26345440, gi|26349141, gi|26349459,
49	1.42	Peptidylprolyl isomerase A	17960	gi|71051228
103	1.53*	Sorbitol dehydrogenase precursor	40066	gi|1009706
117	3.03	Unnamed protein product	57614	gi|52787

[a] Peak numbers correspond to those in Figure 1. Asterisks indicate significant differences (two-tailed Student's t test, * $P \leq 0.05$, ** $P \leq 0.01$). ***ND, not detected. [b] GI number is simply a series of digits that are assigned consecutively to each sequence record processed by NCBI. The GI system of sequence identifiers runs parallel to the accession.version system, which was implemented by GenBank, EMBL, and DDBJ in February 1999. Therefore, if the protein sequence changes in any way, it will receive a new GI number. (http://www.ncbi.nlm.nih.gov/Sitemap/samplerecord.html#ProteinIDB).

injection loop, and washed using 0.10% TFA in 2.0% acetonitrile at 30 μL/min using the Switchos pump. Peptides were then separated on a nanoflow column (75 μm i.d. × 15 cm, C18 PepMap) at a flow rate of 170 μL/min, employing a gradient from 5.0% to 60% buffer B (0.10% formic acid in 80% acetonitrile) over a period of 35 min (A buffer: 0.10% formic acid in 2.0% acetonitrile). One-second MS/MS scans were performed on each precursor ion. Ions observed with m/z between 350 and 1250 were fragmented with capillary energies from 1300 to 1800 V. The proteins were identified in accord with the previous method.[15,17] There were several candidates with the same score for the unnamed protein products (peak numbers 33 and 45).

Statistical Analysis. Results are expressed as the mean ± SD. The significance of the difference in means was determined by a two-tailed Student's t test.

Results and Discussion

Validation of The FD-LC–MS/MS Method. With the FD-LC–MS/MS method, more than 500 peaks were obtained from an extract of mouse liver tissue derivatized with DAABD-Cl. Typical chromatograms derived from transgenic and non-transgenic mice are depicted in Figure 1. Only the proteins which expression was estimated to fluctuate between transgenic and non-transgenic mice on the same months were identified after isolation, tryptic digestion, and LC–MS/MS identification of arbitrarily selected peak fractions (113 proteins). As a result, 106 proteins differed between transgenic and non-transgenic mice from 6 to 16 months of age, as summarized in Tables 1–3. The total protein amount required for quantification and identification was only 8.0 μg per injection, and identification of even low-abundance proteins was possible with 40 μg of total protein per injection into an HPLC column. In general, proteome analysis of biological samples labeled with CyDye, ICAT, cICAT, or iTRAQ requires from dozens to hundreds of micrograms of protein samples.[3,7–10,11,13,14,28] The accuracy of the method was acquired based on the reproducibility of the peak heights using peaks 53, 83, and 32 as representatives of the high, medium, and low peaks obtained from each individual mouse. The relative standard deviation (RSD, %) for each between-day peak was less than 16 (high peak), 17 (medium peak), and 23% (low peak) (n = 3). The reproducibility of the retention time was also calculated using peak 32. The between-day RSD was 0.41% (n = 3). As an additional benefit, the simple apparatus, consisting of a pump, a column, and a fluorescence detector, does not require a complex facility for operation. In this study, we attempted a comprehensive profiling analysis of an 11-h operation to evaluate the utility of the method. After the elution time of a subject protein has been determined, it will be possible to reduce the analysis time for an arbitrary analysis of the subject protein by re-optimizing the separation conditions. It would also be possible to reduce the overall analysis time if we could develop a higher-performance column.

Table 3. Altered Proteins between Tg and NTg Mouse Livers for 16 Months[a]

peak number	Tg/NTg ratio	protein name	molecular mass (Da)	GI number[b]
		Down-Regulated		
		respiration		
4	0.41	Hemoglobin, β adult major chain	15738	gi|31982300
67	0.69	Hemoglobin β	15653	gi|229301
53	0.70	α-globin	15076	gi|49902
108	0.70	Quininoid dihydropteridine reductase	25554	gi|21312520
		protein synthesis		
101	0.54	Regucalcin	33385	gi|6677739
		defense		
16	0.69	SOD	15955	gi|201006
65	0.64	Manganese superoxide dismutase	24662	gi|53450
40	0.53	Thioredoxin 1	11668	gi|6755911
63	0.72	Glutathione peroxidase (GSHPx-1) (Cellular glutathione peroxidase)	22268	gi|121666
75	0.49*	Glycine *N*-methyltransferase	32712	gi|15679953
79	0.61	Glutathione S-transferase, mu 1	25953	gi|61402231
83	0.69	BHMT	44992	gi|62533211
95	0.61	Glutathione *S*-transferase, α 3	25344	gi|31981724
97	0.51	Chain B, Glutathione *S*-Transferase Yfyf Cys 47-Carboxymethylated Class Pi, Free Enzyme	23350	gi|2624496
		fatty acid metabolism (containing β-oxidation)		
36	0.69	Fatty acid-binding protein, hepatic (fragment)	10173	gi|90485
82	0.58	Acetyl-Coenzyme A acyltransferase 2 (mitochondrial 3-oxoacyl-Coenzyme A thiolase)	41831	gi|20810027
107	0.70	Acetyl-Coenzyme A acyltransferase 1	43926	gi|18700004
85	0.32*	Hydroxyacyl-Coenzyme A dehydrogenase/3-ketoacyl-Coenzyme A thiolase/enoyl-Coenzyme A hydratase (trifunctional protein), β subunit (HADHB)	51353	gi|13542763
102	0.58	Peroxisomal acyl-CoA oxidase	74608	gi|2253380
		apoptosis		
3	0.69	Eukaryotic translation elongation factor 1 α 1	50140	gi|13278382
8	0.58*	Ribosomal protein S29, isoform 1	6672	gi|22267962
		glycolytic system		
61	0.79	Fructose-bisphosphate aldolase B	39548	gi|15723269
98	0.42	Enolase 1, α non-neuron	47095	gi|12963491
99	0.58	Enolase 1, α non-neuron	47095	gi|12963491
		metabolism		
32	0.46**	Cystatin B	11039	gi|6681071
68	0.80	Carbonic anhydrase 3	29348	gi|31982861
72	0.53	Carbonic anhydrase 3	29348	gi|31982861
109	0.30**	PREDICTED: Carbamoyl-phosphate synthetase 1 (CPS1)	165705	gi|51705066
84	0.50	Argininosuccinate synthetase	46555	gi|6996911
		signal transduction		
87	0.65	Electron transferring flavoprotein, α polypeptide	35018	gi|13097375
		amino acid synthesis		
80	0.39	4-Hydroxyphenylpyruvate dioxygenase	45054	gi|849053
		other		
38	0.54	Histidine triad nucleotide binding protein 1	13768	gi|33468857
49	0.71	Peptidylprolyl isomerase A	17960	gi|71051228
64	0.69	Nit protein 2	30483	gi|12963555
86	0.64	γ-actin	40992	gi|809561
96	0.50	Unknown (protein for IMAGE:6414729)	50209	gi|53734652
103	0.70	Sorbitol dehydrogenase precursor	40066	gi|1009706
106	0.68	Heat-responsive protein	18462	gi|1255116
48	0.59	Unnamed protein product	65586	gi|12859782
		Up-Regulated		
		respiration		
37	1.33	α-globin	15076	gi|49900
		fatty acid metabolism (containing β-oxidation)		
35	1.60	Fatty acid-binding protein, hepatic (fragment)	10173	gi|90485
		other		
17	1.30	ND***		
33	1.34	Unnamed protein product	57807, 58587, 57007, 52653	gi|12852157, gi|26345440, gi|2634914, gi|26349459

[a] Peak numbers correspond to those in Figure 1. Asterisks indicate significant differences (two-tailed Student's *t* test, $^{*}P \leq 0.05$, $^{**}P \leq 0.01$). ***ND, not detected. [b] GI number is simply a series of digits that are assigned consecutively to each sequence record processed by NCBI. The GI system of sequence identifiers runs parallel to the accession.version system, which was implemented by GenBank, EMBL, and DDBJ in February 1999. Therefore, if the protein sequence changes in any way, it will receive a new GI number. (http://www.ncbi.nlm.nih.gov/Sitemap/samplerecord.html#ProteinIDB).

Differential Profiling. Differential profiling analysis was performed using liver tissue from HCV core gene transgenic and non-transgenic mice as model samples to evaluate the feasibility of the FD-LC–MS/MS method for clinical proteomics. To investigate the differential expression of proteins in transgenic and non-transgenic mice, the heights of the peaks corresponding to specific retention times were compared for each month of age, with 106 altered proteins observed. The differentially expressed proteins were classified by age, regulation and function (see Tables 1–3). Tg/NTg ratios over 1.2 were defined as up-regulated, and those below 0.8 were defined as down-regulated. Many proteins were up- or down-regulated during the progression of HCV-associated liver disease. Fifteen proteins were significantly altered in their levels of protein contents (Figure 2). At the age of 6 months, there were fewer down-regulated proteins than up-regulated (9 vs 19 proteins). In contrast, many kinds of proteins were different between transgenic- and non-transgenic mice at 12 months, with 11 proteins being down-regulated and 65 being up-regulated. At 16 months, there were more down-regulated proteins than in any other months (39 proteins), but only a small minority (four) of proteins were up-regulated.

The remarkable decrease in major urinary protein (MUP) and eukaryotic translation elongation factor 1 α 1 (EF-1α1) seen in Figure 2a represents an early event in the progression of HCV-associated liver disease (at 6 months). MUP has been known as a negative tumor marker.[23] Suppression of EF-1α1 expression prevents the induction of apoptosis, with the regulation reflected in an antiapoptotic mode.[24] Although one of the α-globin peaks (peak no. 52) decreased significantly, the other three peaks of α-globin (peak nos. 27, 29, and 37) tended to increase (see Table 1). The expression of α-globin has been shown to be up-regulated in apoptotic stimuli.[25] Therefore, the phenomenon might be considered a trend in apoptosis at this stage. Another observation made at the age of 6 months was the up-regulation of enzymes related to β-oxidation.

At 12 months of age, proteins related to respiration, the electron-transfer system, and defense against reactive oxygen species (ROS) were significantly up-regulated (Figure 2b). Moreover, a majority of proteins involved in respiration, protein synthesis, defense, apoptosis, the glycolytic system, and metabolism were more up-regulated than the changes observed at 6 months (Table 2).

Finally, at 16 months, proteins related to defense, β-oxidation, and apoptosis significantly decreased. Cystatin B[26] and carbamoyl-phosphate synthetase 1 (CPS1)[27] are known to be down-regulated in tumor and/or carcinoma and exhibited a significant decrease with the proposed method (Figure 2c). It was also established that various biological functions such as respiration, protein synthesis, defense, and metabolism tended to decline (Table 3).

As a whole, the investigation of the differential expression of proteins in transgenic and non-transgenic mice revealed that many proteins related to biological functions such as respiration, protein synthesis, defense, β-oxidation, and apoptosis fluctuate during the progression of chronic hepatitis C. These changes may reflect a gross effect derived from the loss of liver function in the various stages of chronic hepatitis in HCV infection.

Additionally, these data support, from the viewpoint of proteomics, the former results obtained from morphological and biochemical observation.[19–21] For example, previous reports suggested that HCV core protein might affect a specific pathway in the lipid metabolism.[19,21] In fact, the core protein has a specific effect on lipid metabolism; fat droplets are formed and accumulate in the liver, leading to steatosis. An analysis of the composition of these lipid droplets determined that the concentration of carbon 18 monosaturated (C18:1) fatty acids, such as oleic and vaccenic acid, significantly increased in the livers of transgenic mice as well as in chronic hepatitis C patients.[21] In the present study, hydroxyacyl-Coenzyme A dehydrogenase/3-ketoacyl-Coenzyme A thiolase/enoyl-Coenzyme A hydratase (trifunctional protein) β subunit (HADHB), which catalyzes fatty-acid metabolism, significantly decreased after 16 months (Figure 2). However, at 12 months, other enzymes associated with β-oxidation tended to increase (Table 2: peak nos. 7 and 82). In addition, up-regulation of ATP synthase led to an increase in the synthesis and metabolism of fatty acid at 12 months (Figure 2). Furthermore, acetaldehyde dehydrogenase (ALDH), which catalyzes the acetaldehyde metabolism, tended to be up-regulated in the same month (Figure 2). The metabolic reactions of fatty acid and acetaldehyde generate $NADH_2^+$, and the overexpression then causes suppression of both metabolisms. Hence, these results suggest that the fatty-acid metabolism may become milder and resulted from the multiple protein changes related to β-oxidation, ATP synthase, and acetaldehyde metabolism with the progression of HCV-associated liver disease.

Previous reports also suggested that HCV core protein might alter the oxidant/antioxidant state in the liver.[20] The reports demonstrated that there is no significant difference in the levels of lipid peroxidation at 3 and 12 months of age, resulting in cellular and tissue damage by ROS. In contrast, after 16 months, the peroxidation and hydrogen peroxide levels increased remarkably and the levels of total and reduced glutathione, which plays an important role as an antioxidant, decreased. While, our results demonstrate that enzymes related to the antioxidant effect, such as betaine-homocysteine methyltransferase (BHMT) and Cu/Zn-superoxide dismutase (SOD), were up-regulated in transgenic mice at 12 months (Table 2: defense). Subsequently, up to 16 months, a decrease in BHMT and glycine *N*-methyltransferase related to the methylation cycle was observed (Figure 2). The decrease in these enzymes led to a deficiency of adenosylmethionine, impairing mitochondrial function and generating oxidative stress in the liver.[29,30] It has recently been shown that a chronic deficiency of adenosylmethionine in the liver results in the spontaneous progression of steatohepatitis and HCC.[31] In addition, the down-regulation of glycine *N*-methyltransferase would inhibit the synthesis of glutathione resulting in a shift to the oxidizing state, thereby reducing cell proliferation and increasing apoptosis.[32] Therefore, the observed expression of antioxidants might reflect direct oxidative stress status; although at 12 months the up-regulated antioxidants protected against oxidative stress, the oxidative stress might become dominant by the deficiency of antioxidants among the progression of liver disease. Also, these results, derived from both studies, strongly suggest that HCV core protein induces ROS in an age-dependent manner. After 16 months, a biochemical[20] and proteomic analysis revealed a lack of glutathione, suggesting that supplying glutathione might be more effective than SOD in the progression of HCC in the late stage. Although a further animal experiment should be required for reliable clarification of the hepatocarcinogenesis mechanism, the proposed method was demonstrated to be extremely

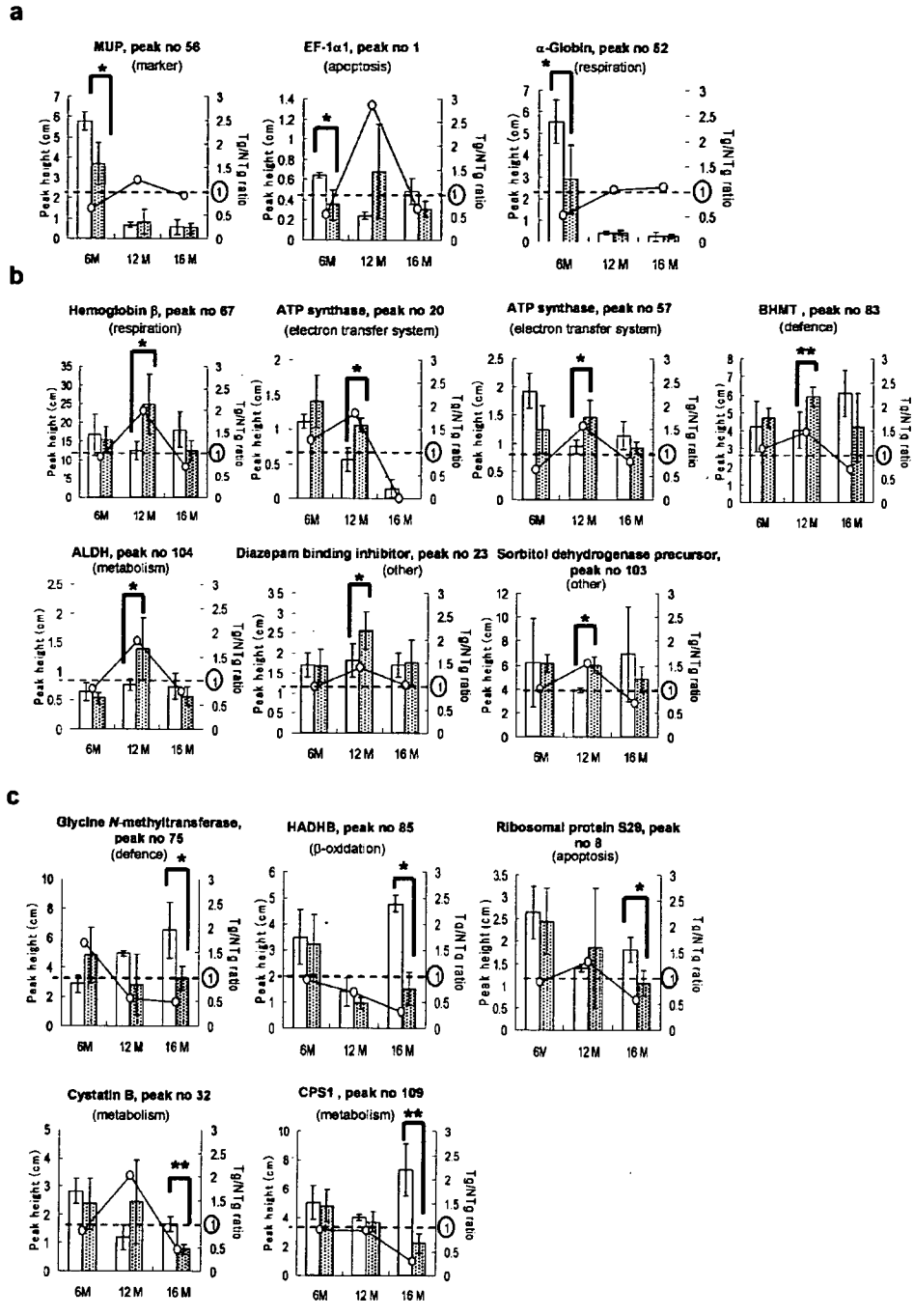

Figure 2. Comparison of peak heights between transgenic (Tg; gray bar) and non-transgenic (NTg; white bar) mice, and the Tg-to-NTg ratio (open circle) from 6 months (6M) to 16 months (16M). Significantly altered proteins are seen at 6M (a), 12M (b), and 16M (c). Peak numbers correspond to those in Figure 1. Mean values ± SD are plotted. Asterisks indicate significant differences (two-tailed Student's *t* test of all data points, $*P \leq 0.05$, $**P \leq 0.01$).

useful for understanding biotransformation from the viewpoint of proteomics. Also, the data obtained in this experiment could support the understanding of hepatocarcinogenesis with HCV infection in terms of proteomics in addition to the morphological and biochemical observations mentioned above.

Conclusions

The proposed method demonstrated for the first time the existence of several event-marker proteins at the three progression stages of hepatocarcinogenesis in transgenic mice. It should be stressed that the FD-LC–MS/MS method would also

be worthwhile for clinical proteomics analysis, as a supplement to gel- and LC-based methods.

Acknowledgment. We thank Mr. Itaru Yazawa, Imtakt Co., for supplying Intrada WP-RP and Cadenza CL-C18 columns. Part of the work was supported by MEXT-HAITEKU (2004–2008).

References

(1) Romijin, E. P.; Krijgsveld, J.; Heck, A. J. R. Recent liquid chromatographic-(tandem) mass spectrometric applications in proteomics. *J. Chromatogr., A.* **2003**, *1000* (1–2), 589–608.
(2) Figeys, D. Proteomics in 2002: A year of technical development and wide-ranging applications. *Anal. Chem.* **2003**, *75* (12), 2891–2905.
(3) Wu, W. W.; Wang, G.; Baek, S. J; Shen, R. F. Comparative study of three proteomic quantitative methods, DIGE, cICAT, and iTRAQ, using 2D gel- or LC-MALDI TOF/TOF. *J. Proteome Res.* **2006**, *5* (3), 651–658.
(4) Alaoui-jamali, M. A.; Xu, Y. Proteomic technology for biomarker profiling in cancer: an update. *J Zhejiang Univ. Sci. B* **2006**, *7* (6), 411–420.
(5) Fountoulakis, M.; Suter, L. Proteomic analysis of the rat liver. *J. Chromatogr., B* **2002**, *782*, 197–218.
(6) Yokoyama, Y.; Kuramitsu, Y.; Takashima, M.; Iizuka, N.; Toda, T.; Terai, S.; Sakaida, I.; Oka, M.; Nakamura, K.; Okita, K. Proteomic profiling of proteins decreased in hepatocellular carcinoma from patients infected with hepatitis C virus. *Proteomics* **2004**, *4* (7), 2111–2116.
(7) Chromy, B. A.; Gonzales, A. D.; Perkins, J.; Choi, M. W.; Corzett, M. H.; Chang, B. C.; Corzett, C. H.; McCutchen-Maloney, S. L. Proteomic analysis of human serum by two-dimensional differential gel electrophoresis after depletion of high-abundant proteins. *J. Proteome Res.* **2004**, *3* (6), 1120–1127.
(8) Unlu, M.; Morgan, M. E.; Minden, J. S. Difference gel electrophoresis: A single gel method for detecting changes in protein extracts. *Electrophoresis* **1997**, *18* (11), 2071–2077.
(9) Fujii, K.; Kondo, T.; Yokoo, H.; Okano, T.; Yamada, M.; Yamada, T.; Iwatsuki, K.; Hirohashi, S. Database of two-dimensional polyacrylamide gel electrophoresis of proteins labeled with CyDye DIGE Fluor saturation dye. *Proteomics* **2006**, *6* (5), 1640–1653.
(10) Shaw, J.; Rowlinson, R.; Nickson, J.; Stone, T.; Sweet, A.; Williams, K.; Tonge, R. Evaluation of saturation labelling two-dimensional difference gel electrophoresis fluorescent dyes. *Proteomics* **2003**, *3* (7), 1181–1195.
(11) Welch, K. D.; Wen, B.; Goodlett, D. R.; Yi, E. C.; Lee, H.; Reilly, T. P.; Nelson, S. D.; Pohl, L. R. Proteomic identification of protential susceptibility factors in drug-induced liver disease. *Chem. Res. Toxicol.* **2005**, *18* (6), 924–933.
(12) Hansen, K. C.; Schmitt-Ulms, G.; Chalkley, R. J.; Hirsch, J.; Baldwin, M. A.; Burlingame, A. L. Mass spectrometric analysis of protein mixtures at low levels using cleavable ^{13}C-isotope-coded affinity tag and multidimensional chromatography. *Mol. Cell. Proteomics* **2003**, *2* (5) 299–314.
(13) Qu, J.; Jusko, W. J.; Straubinger, R. M. Utility of cleavable isotope-coded affinity-tagged reagents for quantification of low-copy proteins induced by methylprednisolone using lipid chromatography/tandem mass spectrometry. *Anal. Chem.* **2006**, *78* (13), 4543–4552.
(14) Hirsch, J.; Hansen, K. C.; Choi, S.; Noh, J.; Hirose, R.; Roberts, J. P.; Matthay, M. A.; Burlingame, A. L.; Maher, J. J.; Niemann, C. U. Warm ischemia-induced alterations in oxidative and inflammatory proteins in hepatic kupffer cells in rats. *Mol. Cell. Proteomics* **2006**, *5* (6), 979–986.
(15) Masuda, M.; Saimaru, H.; Takamura, N.; Imai, K. An improved method for proteomics studies in *C. elegans* by fluorogenic derivatization, HPLC isolation, enzymatic digestion and liquid chromatography-tandem mass spectrometric identification. *Biomed. Chromatogr.* **2005**, *19* (7), 556–560.
(16) Asamoto, H.; Ichibangase, T.; Saimaru, H.; Uchikura, K.; Imai, K. Existence of low molecular weight thiols in *Caenorhabditis elegans* demonstrated by HPLC-fluorescenece detection utilizing 7-chloro-*N*-[2-(dimethylamino)ethyl]-2,1,3-benzoxadiazole-4-sulfonamide (DAABD-Cl). *Biomed. Chromatogr.* In press.
(17) Masuda, M.; Toriumi, C.; Santa, T.; Imai, K. Fluorogenic derivatization reagents suitable for isolation and identification of cysteine-containing proteins utilizing high-performance liquid chromatography-tandem mass spectrometry. *Anal. Chem.* **2004**, *76* (3), 728–735.
(18) Toriumi, C.; Imai, K. An identification method for altered proteins in tissues utilizing fluorescence derivatization, liquid chromatography, tandem mass spectrometry, and a database searching algorithm. *Anal. Chem.* **2003**, *75* (15), 3725–3730.
(19) Moriya, K.; Yotsuyanagi, H.; Shintani, Y.; Fujie, H.; Ishibashi, K.; Matsuura, Y.; Miyamura, T.; Koike, K. Hepatitis C virus core protein induces hepatic steatosis in transgenic mice. *J. Gen. Virol.* **1997**, *78* (7), 1527–1531.
(20) Moriya, K.; Nakagawa, K.; Santa, T.; Shintani, Y.; Fujie, H.; Miyoshi, H.; Tsutsumi, T.; Miyazawa, T.; Ishibashi, K.; Horie, T.; Imai, K.; Todoroki, T.; Kimura, S.; Koike, K. Oxidative stress in the absence of inflammation in a mouse model for hepatitis C virus-associated hepatocarcinogenesis. *Cancer Res.* **2001**, *61* (11), 4365–4370.
(21) Moriya, K.; Todoroki, T.; Tsutsumi, T.; Fujie, H.; Shintani, Y.; Miyoshi, H.; Ishibashi, K.; Takayama, T.; Makuuchi, M.; Watanabe, K.; Miyamura, T.; Kimura, S.; Koike, K. Increase in the concentration of carbon 18 monounsaturated fatfy acids in the liver with hepatitis C: analysis in transgenic mice and humas. *Biochem. Biophys. Res. Commun.* **2001**, *281* (5), 1207–1212.
(22) Moriya, K.; Fujie, H.; Shintani, Y.; Yotsuyanagi, H.; Tsutsumi, T.; Ishibashi, K.; Matsuura, Y.; Kimura, S.; Miyamura, T.; Koike, K. The core protein of hepatitis C virus induces hepatocellular carcinoma in transgenic mice. *Nat. Med.* **1998**, *4* (9), 1065–1067.
(23) Dragani, T. A; Manenti, G.; Sacchi, M. R. M.; Colombo, B. M.; Della, P. G. Major urinary protein as a negative tumor maker in mouse hepatocarcinogenesis. *Mol. Carcinog.* **1989**, 2 (6), 355–360.
(24) Ejiri, S. Moonlighting functions of polypeptide elongation factor 1: From actin bundling to zinc finger protein R1-associated nuclear localization. *Biosci. Biotechnol. Biochem.* **2002**, *66* (1), 1–21.
(25) Brecht, K.; Simonen, M.; Heim, J. Upregulation of alpha globin promotes apoptotic cell death in the hematopoietic cell line FL5.12. *Apoptosis* **2005**, *10* (5), 1043–1062.
(26) Shiraishi, T.; Mori, M.; Tanaka, S.; Sugimachi, K.; Akiyoshi, T. Identification of cystatin B in human esophageal carcinoma, using differential displays in which the gene expression is related to lymph-node metastasis. *Int. J. Cancer.* **1998**, *79* (2), 175–178.
(27) Wu, S.; Li, S.; Zhang, H.; Luo, J.; Yu, Y. Cloning of cDNA coding for carbamoyl phosphate synthetase 1 and changes in levels of CPS1 mRNA during hepatocarcinogenesis. *Sci. Sin., Ser. B* **1988**, *31* (2), 197–203.
(28) Wilson, K. E.; Marouga, R.; Prime, J. E.; Pashby, D. P.; Orange, P. R.; Crosier, S.; Keith, A. B.; Lathe, R.; Mullins, J.; Estibeiro, P.; Bergling, H.; Hawkins, E.; Morris, C. M. Comparative proteomic analysis using samples obtained with laser microdissection and saturation dye labelling. *Proteomics* **2005**, *5* (15), 3851–3858.
(29) Liang, C. R. M. Y.; Leow, C. K.; Neo, J. C. H.; Tan, G. S.; Lo, S. L.; Lim, J. W. E.; Seow, T. K.; Lai, P. B. S.; Chung, M. C. M. Proteome analysis of human hepatocellular carcinoma tissues by two-dimensional difference gel electrophoresis and mass spectrometry. *Proteomics* **2005**, *5* (8), 2258–2271.
(30) Heil, S. G.; Lievers, K. J.; Boers, G. H.; Verhoef, P.; Den-Heijer, M.; Trijbels, F. J.; Blom, H. J. Betaine-homocysteine methyltransferase (BHMT): Genomic sequencing and relevance to hyperhomocysteinemia and vascular disease in humans. *Mol. Genet. Metab.* **2000**, *71* (3), 511–519.
(31) Santamaria, E.; Avila, M. A.; Latasa, M. U.; Rubio, A.; Martin-Duce, A.; Lu, S. C.; Mato, J. M.; Corrales, F. J. From the cover: Functional proteomics of nonalcoholic steatohepatitis: Mitochondrial proteins as targets of S-adenosylmethionine. *Proc. Natl. Acad. Sci. U.S.A.* **2003**, *100* (6), 3065–3070.
(32) Wu, G.; Fang, Y. Z.; Yang, S.; Lupton, J. R.; Turner, N. D. Glutathione metabolism and its implications for health. *J. Nutr.* **2004**, *134* (3), 489–492.

PR070094C

Int. J. Cancer: **122**, 124–131 (2008)

Hepatitis C virus core protein induces spontaneous and persistent activation of peroxisome proliferator-activated receptor α in transgenic mice: Implications for HCV-associated hepatocarcinogenesis

Naoki Tanaka[1,2]*, Kyoji Moriya[3], Kendo Kiyosawa[2], Kazuhiko Koike[3] and Toshifumi Aoyama[1]

[1]*Department of Metabolic Regulation, Institute on Aging and Adaptation, Shinshu University Graduate School of Medicine, Matsumoto, Japan*
[2]*Division of Gastroenterology, Department of Internal Medicine, Shinshu University School of Medicine, Matsumoto, Japan*
[3]*Department of Internal Medicine, Graduate School of Medicine, University of Tokyo, Tokyo, Japan*

Persistent infection of hepatitis C virus (HCV) can lead to a high risk for hepatocellular carcinoma (HCC). HCV core protein plays important roles in HCV-related hepatocarcinogenesis, because mice carrying the core protein exhibit multicentric HCCs without hepatic inflammation and fibrosis. However, the precise mechanism of hepatocarcinogenesis in these transgenic mice remains unclear. To evaluate whether the core protein modulates hepatocyte proliferation and apoptosis *in vivo*, we examined these parameters in 9- and 22-month-old transgenic mice. Although the numbers of apoptotic hepatocytes and hepatic caspase 3 activities were similar between transgenic and nontransgenic mice, the numbers of proliferating hepatocytes and the levels of numerous proteins such as cyclin D1, cyclin-dependent kinase 4 and c-Myc, were markedly increased in an age-dependent manner in the transgenic mice. This increase was correlated with the activation of peroxisome proliferator-activated receptor α (PPARα). In these transgenic mice, spontaneous and persistent PPARα activation occurred heterogeneously, which was different from that observed in mice treated with clofibrate, a potent peroxisome proliferator. We further demonstrated that stabilization of PPARα through a possible interaction with HCV core protein and an increase in nonesterified fatty acids, which may serve as endogenous PPARα ligands, in hepatocyte nuclei contributed to the core protein-specific PPARα activation. In conclusion, these results offer the first suggestion that HCV core protein induces spontaneous, persistent, age-dependent and heterogeneous activation of PPARα in transgenic mice, which may contribute to the age-dependent and multicentric hepatocarcinogenesis mediated by the core protein.
© *2007 Wiley-Liss, Inc.*

Key words: cell-cycle regulator; peroxisome; nuclear stabilization; heterogeneous PPARα activation

Hepatitis C virus (HCV) is one of the major causes of chronic hepatitis, and persistent infection with this virus can lead to a high incidence of hepatocellular carcinoma (HCC).[1,2] The prevalence of HCC because of chronic HCV infection has increased over the past two decades,[3,4] and chronic HCV infection has therefore been recognized as a serious disease. However, the precise mechanism of hepatocarcinogenesis during chronic HCV infection remains unclear.

Many experiments using cell culture systems have suggested the possibility that HCV core protein itself can modulate various cellular functions and can be directly linked to the development of HCV-related HCC.[5] For example, HCV core protein transforms rat embryo fibroblasts to a tumorigenic phenotype in cooperation with the H-*ras* oncogene,[6] suppresses *c-myc*-related apoptosis[7] and transcription of the *p53* gene,[8] interacts with a variety of proteins, including helicase, lymphotoxin-β receptor, or dead box protein, and modulates their functions.[9] We further established transgenic mouse lines carrying the HCV core gene, in which the core protein is constitutively expressed in the liver at levels similar to that found in chronic hepatitis C patients.[10] These mice exhibited multicentric hepatic adenomas, and developed HCCs in an age-dependent manner.[11] The livers of these mice were almost free of inflammation, necrosis and fibrosis,[10,11] suggesting that the core protein itself has a hepatocarcinogenic potential *in vivo*. However, the molecular mechanism of the development of HCC in the transgenic mice has not been fully understood.

In the livers of HCV core gene transgenic mice, an age-dependent increase in oxidative stress and resultant DNA damage were found,[12] and these effects may contribute to or facilitate the development of HCC. Another possible mechanism of hepatocarcinogenesis is continuous enhancement of hepatocyte proliferation. Cell proliferation and apoptosis are highly regulated processes for maintaining homeostasis in many organs, and during the carcinogenic process, sustained imbalance generally precedes cancer.[13,14] For example, in patients with chronic HCV infection, high hepatocyte proliferative activity relative to apoptosis may reliably predict a new development of HCC.[15] However, there is no information about whether or not hepatocyte proliferation accelerates persistently in mice carrying the HCV core gene, and no information about how the core protein promotes hepatocyte proliferation *in vivo*. In the current study, we began to examine changes in the parameters of hepatocyte proliferation and apoptosis in the transgenic mice.

Material and methods

Animals and treatments

HCV core gene transgenic mice on a C57BL/6N genetic background were produced as described earlier.[10] Because HCC developed preferentially in male transgenic mice,[11] 9- and 22-month-old male mice ($n = 8$ for either age group) were adopted. Sex- and age-matched nontransgenic mice ($n = 8$ for either age group) were used as controls. These mice were fed an ordinary diet and were treated in a specific pathogen-free state according to the institutional guidelines. For additional experiment, male wild-type mice fed a control diet containing 0.5% clofibrate for 2 weeks ($n = 8$) were used. All mice were killed by cervical dislocation and the livers were excised. When a hepatic tumor was present, it was removed and the remaining liver tissue was used. All experiments were performed in accordance with animal study protocols approved by the Shinshu University School of Medicine.

Abbreviations: AOX, acyl-CoA oxidase; CDK, cyclin-dependent kinase; DAB, 3,3'-diaminobenzidine; FITC, fluorescein isothiocyanate; HCC, hepatocellular carcinoma; HCV, hepatitis C virus; L-FABP, liver-type fatty acid-binding protein; NEFA, nonesterified fatty acid; PBS, phosphate-buffered saline; PCNA, proliferating cell nuclear antigen; PMSF, phenylmethylsulfonyl fluoride; PPAR, peroxisome proliferator-activated receptor; PT, peroxisomal thiolase; RXR, retinoid X receptor; SDS, sodium dodecyl sulfate; TUNEL, terminal deoxynucleotidyl transferase-mediated deoxyuridine triphosphate nick-end labeling.

***Correspondence to:** Department of Metabolic Regulation, Institute on Aging and Adaptation, Shinshu University Graduate School of Medicine, 3-1-1 Asahi, Matsumoto, 390-8621, Japan. Fax: +81-26-337-3094.
E-mail: naopi@hsp.md.shinshu-u.ac.jp
Received 2 May 2007; Accepted after revision 28 June 2007
DOI 10.1002/ijc.23056
Published online 31 August 2007 in Wiley InterScience (www.interscience.wiley.com).

Preparation of hepatocyte nuclear fraction

Approximately 200 mg of liver tissues was transferred to a chilled Dounce homogenizer (Wheaton, Milliville, NJ) and homogenized on ice by 30 strokes in 1.2 mL of nuclei buffer [300 mM sucrose in 10 mM Tris-HCl, pH 7.4, 15 mM NaCl, 5 mM $MgCl_2$ and 0.25 mM phenylmethylsulfonyl fluoride (PMSF)]. The homogenate was filtered through gauze and centrifuged at 4,500*g* for 5 min at 4°C. The resulting pellet was resuspended, layered over 2 mL of nuclei buffer containing 2 M sucrose, and centrifuged at 23,000*g* for 1 hr at 4°C. The pellet obtained after ultracentrifugation was resuspended in 250 μL of nuclei buffer and used as the nuclear fraction. Preparation of nuclear fraction from isolated hepatocytes was performed as described elsewhere.[16]

Immunoblot analysis

Protein concentration was measured colorimetrically by a BCA™ Protein Assay kit (Pierce, Rockford, IL). For analysis of fatty acid-metabolizing enzymes and protein, whole liver lysate (10–20 μg protein) was subjected to 10% sodium dodecyl sulfate (SDS)-polyacrylamide gel electrophoresis.[17] For analysis of other proteins, hepatocyte nuclear fraction (100 μg protein) or whole liver lysate (200–300 μg protein) was subjected to electrophoresis. After electrophoresis, the proteins were transferred to nitrocellulose membranes, which were incubated with the primary antibody, followed by alkaline phosphatase-conjugated goat anti-rabbit or anti-mouse IgG. The origin of the primary rabbit polyclonal antibodies against fatty acid-metabolizing enzymes and protein was described earlier.[17] For immunoblot analysis of peroxisome proliferator-activated receptor α (PPARα), a polyclonal anti-mouse antibody[18] or commercial antibody (Santa Cruz Biotechnology, Santa Cruz, CA) was used. The antibodies against cell-cycle regulators and oncogene products were purchased commercially (Santa Cruz Biotech.).[19] Equal loading of the protein obtained from whole liver lysate and nuclear fraction was confirmed by reprobing the membranes with an antibody against β-actin and histone H1, respectively. The band intensity of nuclear PPARα was quantified densitometrically, normalized to that of histone H1, and subsequently expressed as the fold changes relative to that of 9-month-old nontransgenic mice.

mRNA analysis

Total liver RNA was extracted with an RNeasy Mini Kit™ (Qiagen, Valencia, CA). Five microgram of RNA was electrophoresed on 1.1 M formaldehyde-containing 1% agarose gels and transferred to nylon membranes by capillary blotting in 20× SSC buffer (3 M NaCl and 300 mM sodium citrate, pH 7.0) overnight. The membranes were hybridized with ^{32}P-labeled cDNA probes. The blots were exposed to a phosphorimager screen cassette and were analyzed using a Molecular Dynamics Storm 860 Phosphorimager system (Sunnyvale, CA). The origin of the cDNA probes has been described elsewhere.[17–19] Northern blot of β-actin was used as the internal control. The blot intensity was quantified, normalized to that of β-actin and subsequently expressed as the fold changes relative to that of 9-month-old nontransgenic mice.

Pulse-label and pulse-chase experiment

Parenchymal hepatocytes were isolated from transgenic and control mice by the modified *in situ* perfusion method.[20] After perfusion with 0.05% collagenase solution (Wako, Osaka, Japan), the isolated hepatocytes were washed thrice by means of differential centrifugation and the dead cells removed by density gradient centrifugation on Percoll (Amersham Pharmacia Biotech, Buckinghamshire, UK). The live hepatocytes were washed and suspended in William's E medium containing 5% fetal bovine serum. When the viability of the isolated hepatocytes exceeded 85% as determined by the trypan blue exclusion test, the following experiments were conducted. The isolated hepatocytes were washed twice and incubated in methionine-free medium containing 5% dialyzed fetal bovine serum for 1 hr at 37°C. The medium was replaced with the same medium containing 300 μCi/mL of [^{35}S]methionine (Amersham Pharmacia Biotech.). After 3-hr of incubation, the labeled medium was changed to the standard medium and the preparation was chased for 4, 8 or 16 hr. The labeled cells were washed, homogenized and centrifuged for preparation of the nuclear fraction. The levels of radioactivity in the homogenates of the pulse-labeled preparations were similar between the transgenic and the nontransgenic mice, suggesting that the [^{35}S]methionine uptake capacity in the former hepatocytes is similar to that in the latter. The nuclear fraction was lysed in RIPA buffer [10 mM Tris-HCl, pH 7.4, 0.2% sodium deoxycholate, 0.2% Nonidet P-40, 0.1% SDS, 0.25 mM PMSF, 10 μg/mL aprotinin]. The lysate was incubated for 3 hr at 4°C with purified anti-PPARα antibody. The immune complexes were precipitated with *Staphylococcus aureus* protein A bound to agarose beads. After the precipitates had been washed in RIPA buffer, the labeled proteins were resolved by 10% SDS-polyacrylamide gel electrophoresis and visualized by autoradiography. The nuclear fractions of the pulse-labeled preparations were also used for immunoblot analysis of PPARα.

Affinity chromatography for PPARα complex

All procedures were performed at 4°C. The nuclear fraction from the mouse liver was mixed with a 4-fold volume of a solution containing 12.5 mM potassium phosphate, pH 7.5, 25 mM NaCl, 0.25% Tween 20 and 0.1 mM PMSF. The mixture was briefly sonicated with a microsonicator, the Powersonic Model 50 (Yamato, Tokyo, Japan), and then centrifuged at 100,000*g* for 20 min. The supernatant was applied to an immobilized anti-PPARα IgG column (1.0 × 4.0 cm^2), prepared with the Affigel HZ Immunoaffinity kit® (Bio-Rad, Hercules, CA) and equilibrated with 10 mM potassium phosphate, pH 7.5, 20 mM NaCl and 0.2% Tween 20. The solution was again passed through the column and this was repeated at least thrice. The column was washed and the elution performed with 150 mM sodium citrate, pH 3.0, and 200 mM NaCl, in a total volume of 2 mL. The eluate was resolved by 10 and 15% SDS-polyacrylamide gel electrophoresis for PPARα and the HCV core protein, respectively. The core protein expressed in COS cells was used as a positive marker.[21] The monoclonal antibody against the core protein was purchased commercially (ViroGen, Watertown, MA).

Cytochemical staining of peroxisomes

Liver peroxisome proliferation was evaluated by using 3,3′-diaminobenzidine (DAB) staining for catalase according to the method of Novikoff and Goldfischer with minor modifications.[22] Small pieces of liver were fixed with 2% glutaraldehyde in 100 mM sodium cacodylate buffer, pH 7.2, for 3 hr at 4°C, rinsed with sodium cacodylate buffer and cut into 100-μm sections with a Lancer® Vibratome 1000 (Lancer, Bridgeton, MO). These sections were then incubated for 1 hr at 37°C in the DAB reaction medium (0.2% DAB tetrahydrochloride in 50 mM propanediol, pH 9.7, 5 mM KCN, 0.05% H_2O_2) and postfixed with 1% OsO_4 in 100 mM sodium phosphate, pH 7.4 for 1 hr. The sections were dehydrated through a graded series of ethanol and acetone treatments and embedded in Epok 812 (Oken, Tokyo, Japan). One micrometer sections were prepared, counterstained with 0.1% toluidine blue solution and examined by light microscopy. For electron microscopic examination, 0.1-μm sections were cut with a diamond knife, collected on grid meshes, stained with lead citrate and uranyl acetate and visualized with a JEM 1200EX II electron microscope (JEOL, Tokyo, Japan) at an accelerating voltage of 80 keV.

Morphometry of hepatic peroxisomes

Morphometric analysis of DAB-stained peroxisomes was carried out using electron photomicrographs. For each mouse, 10 independent fields in the pericentral area of liver lobuli were photomicrographed at an original magnification of 4,000×. At this magnification, peroxisomes smaller than 450 nm were clearly

identified. Peroxisomes were easily detected because of their high contrast because of the positive DAB reaction. In each frame, the number of peroxisomal profiles and the area of each individual profile were determined. The numerical density and volume density of peroxisomes were calculated using the following equations: numerical density (number/μm^2) = $N_P/(A_T - A_{empty})$, and volume density (%) = $A_{TP}/(A_T - A_{empty}) \times 100$, where N_P is the peroxisome number in the test area, A_T is the test area, A_{empty} is the area of the vascular and biliary lumens and that of the hepatocyte nuclei and lipid droplets, and A_{TP} is the area of total peroxisomal profiles in the test area. The area was measured with a Luzex AP image analyzer (Nireco, Tokyo, Japan).

Immunofluorescence staining

Liver samples were fixed in 4% paraformaldehyde in phosphate-buffered saline (PBS), embedded in Tissue-Tek O.C.T compound™ (Sakura Finetek, Torrance, CA) and frozen. Frozen liver 5-μm sections were prepared, washed with PBS, blocked with bovine serum albumin for 1 hr and incubated overnight with rabbit polyclonal antibodies against cyclin D1 (1:50 dilution)[19] and PPARα (1:100 dilution),[18] and with mouse monoclonal antibody against proliferating cell nuclear antigen (PCNA) (1:100 dilution).[19] After 5 washes with PBS, these sections were incubated with fluorescein isothiocyanate (FITC)-conjugated goat anti-rabbit IgG (Jackson ImmunoResearch, West Grove, PA) or donkey anti-mouse IgG (Dako). The sections were mounted and viewed with an Olympus Fluoview confocal laser scanning microscope (Olympus, Tokyo, Japan). Two-thousand hepatocyte nuclei were examined for each mouse, and the number of hepatocyte nuclei stained with the antibodies against cyclin D1, PPARα and PCNA was counted and expressed as a percentage.

Assessment of apoptotic hepatocytes

Liver samples were cut into small pieces and then fixed in 4% paraformaldehyde in PBS. These samples were dehydrated, embedded in paraffin and cut into 4-μm sections. The terminal deoxynucleotidyl transferase-mediated deoxyuridine triphosphate nick-end labeling (TUNEL) assay was performed using a MEBSTAIN Apoptosis Kit II (Medical and Biological Laboratories, Nagoya, Japan). The number of apoptotic hepatocytes in 2,000 hepatocytes was counted for each mouse, and expressed as a percentage.

Other methods

Hepatic caspase 3 activity was measured as described elsewhere.[23] For analysis of the nuclear contents of nonesterified fatty acids (NEFAs), ~150 μL of the hepatocyte nuclear fraction, containing 1–2 mg of protein, was treated with a microsonicator. Lipid extraction was performed according to a modification of the method developed by Folch *et al.*[24] and the nuclear content of NEFAs was measured with a *NEFA* C-test kit™ (Wako).

Statistical analysis

Statistical analysis was performed by means of Student's *t*-test. The results are expressed as the mean ± standard deviation. A probability value of less than 0.05 was considered to be statistically significant.

Results

Accelerated hepatocyte proliferation in HCV core gene transgenic mice

To evaluate hepatocyte proliferative activity, PCNA-positive hepatocytes were counted in male transgenic mice and nontransgenic mice. Although hepatic inflammation and hepatocyte necrosis were not detected in either group, the numbers of PCNA-positive hepatocytes were significantly increased in the 9-month-old transgenic mice compared with the 9-month-old nontransgenic mice (Fig. 1*a*). The increase was more significant in the

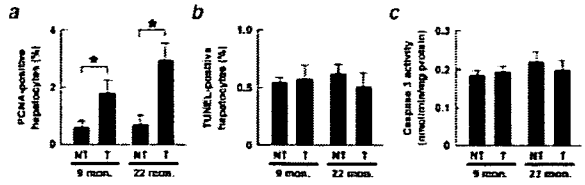

FIGURE 1 – Increase in hepatocyte proliferative activity. (*a*) The number of PCNA-positive hepatocytes. Two-thousand hepatocyte nuclei were examined for each mouse, and the number stained with anti-PCNA antibody was counted. Results are expressed as the mean ± standard deviation ($n = 8$). *, $p < 0.05$ between the transgenic mice and the nontransgenic mice; NT, nontransgenic mice; T, transgenic mice; 9 mon, 9-month-old mice; 22 mon, 22-month-old mice. (*b*) The number of apoptotic hepatocytes. The number of TUNEL-positive hepatocytes in 2,000 hepatocytes was determined for each mouse. Results are expressed as the mean ± standard deviation ($n = 8$). (*c*) Caspase 3 activity. Results are expressed as the mean ± standard deviation ($n = 8$).

22-month-old transgenic mice (Fig. 1*a*). The numbers of PCNA-positive hepatocytes in the 22-month-old transgenic mice corresponded with those in HCV polyprotein-expressing transgenic mice with HCC.[25] On the other hand, the parameters of apoptosis, *i.e.*, the numbers of TUNEL-positive hepatocytes and hepatic caspase 3 activity, remained unchanged between the 2 groups at the same ages (Figs. 1*b* and 1*c*). These results suggest that spontaneous hepatocyte proliferation occurs as early as the age of 9 months and persists for a long time in HCV core gene transgenic mice.

Simultaneous induction of cell-cycle regulators and oncogene products in HCV core gene transgenic mouse livers

To examine the changes in the expression of proteins associated with hepatocyte division, the livers of the 9- and 22-month-old mice were subjected to immunoblot analysis. The levels of many proteins including cell-cycle regulators [cyclin-dependent kinase (CDK) 1, 2 and 4, cyclin D1 and E, and PCNA], and oncogene products (c-Myc, c-Fos and c-Ha-Ras) were significantly higher in the 22-month-old transgenic mice than in the control mice (Fig. 2). The levels of CDK inhibitors such as p16 and p21 were similar between the 2 groups. Similar results were obtained from the 9-month-old transgenic mice (data not shown). Time course changes in the expression of key G1-S checkpoint regulators, cyclin D1 and CDK4, are shown in Figure 3*a*. The simultaneous increase in the expression of cyclin D1 and CDK4 in the transgenic mice was continuous and more pronounced with age. Northern blot analysis revealed that the increase of these proteins occurred at the transcriptional level (Figs. 3*b* and 3*c*). Thus, these results reveal that various proteins which accelerate cell-cycle progression were induced simultaneously, persistently and age-dependently in the transgenic mice.

Correlative induction of PPARα targets in HCV core gene transgenic mouse livers

As shown in Figure 2, the expression of many kinds of cell-cycle regulators and oncogene products is known to be induced by the functional activation of PPARα.[19,26–30] To investigate whether PPARα is activated in the livers of transgenic mice, the expression of representative PPARα target genes,[30] acyl-CoA oxidase (AOX), peroxisomal thiolase (PT) and liver-type fatty acid-binding protein (L-FABP), was examined. As demonstrated in Figure 3*a*, the levels of AOX, PT, and L-FABP were increased in the 9-month-old transgenic mice compared with the nontransgenic mice, and the increase was more pronounced in the 22-month-old transgenic mice. Northern blot analysis demonstrated that the increase in these PPARα targets was based on the increase in the transcriptional activity (Figs. 3*b* and 3*c*). The increase in the

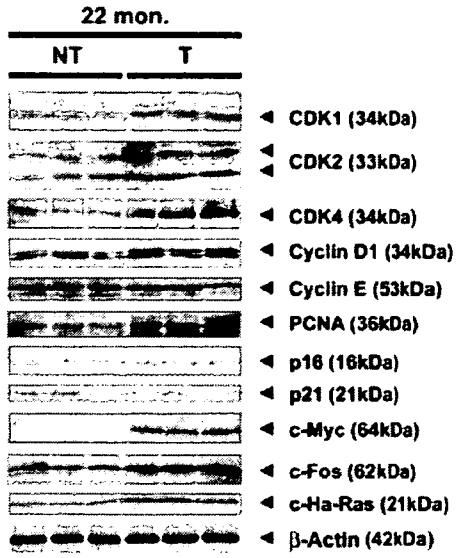

FIGURE 2 – Immunoblot analysis of cell-cycle regulators and oncogene products. Whole liver lysate (200 μg) was loaded in each lane. The band of β-actin was used as the loading control. The apparent molecular weight is indicated in parentheses. 22 mon, 22-month-old mice; NT, nontransgenic mice; T, transgenic mice.

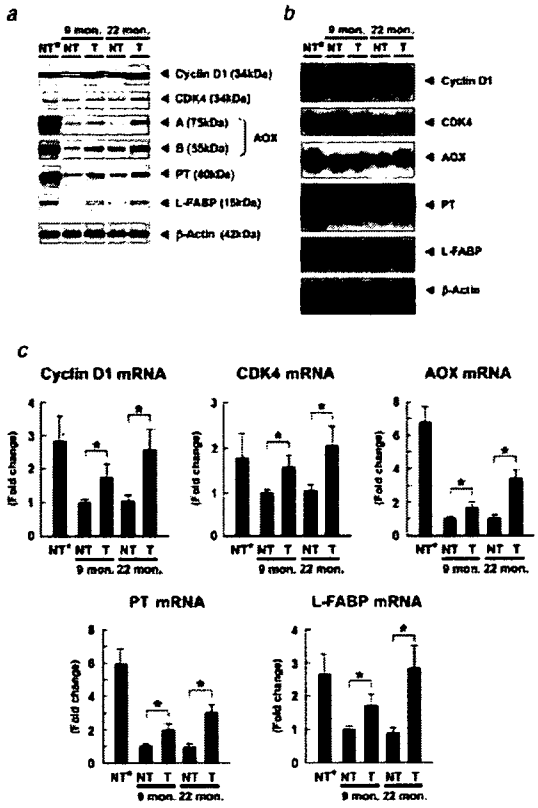

FIGURE 3 – Analysis of PPARα-regulated proteins. (*a*) Immunoblot analysis of cell-cycle regulators and fatty acid-metabolizing enzymes and proteins. Since no significant individual differences in the same mouse group were found in the preliminary experiments, 10 mg of liver pieces prepared from each mouse (n = 8/group) was mixed and homogenized. Whole liver lysate (200 μg for cyclin D1 and CDK4, and 20 μg for others) was loaded in each lane. The band of β-actin was used as the loading control. Results are representative of 4 independent experiments. The apparent molecular weight is indicated in parentheses. 9 mon, 9-month-old mice; 22 mon, 22-month-old mice; NT, nontransgenic mice; T, transgenic mice; NT*, nontransgenic mice treated with a control diet containing 0.5% clofibrate for 2 weeks; A and B, full-length and truncated AOX, respectively. (*b*) Northern blot analysis concerning the proteins in (*a*). Ten milligram of liver pieces from each mouse (n = 8/group) was mixed and homogenized, and total liver RNA was extracted. Hepatic RNA (5 μg) was separated on a denaturing gel, transferred to membranes and hybridized with the indicated ^{32}P-labeled cDNA probes. The blot of β-actin was used as the internal control. Results are representative of 4 independent experiments. (*c*) Quantification of hepatic mRNA levels. The mRNA level was quantified using a phosphorimager, normalized to that of β-actin, and subsequently normalized to that of 9-month-old nontransgenic mice. Results were obtained from 4 independent experiments and expressed as the mean ± standard deviation. Abbreviations are identical with those in (*b*). *, $p < 0.05$ between the transgenic mice and the nontransgenic mice.

mRNA expression of AOX, PT and L-FABP corresponded exactly with that of cyclin D1 or CDK4 (Figs. 3*b* and 3*c*). Therefore, these results demonstrate the strong correlation between continuous and age-dependent induction of cell-cycle regulators and functional activation of PPARα in these transgenic mice. Furthermore, the induction of these 5 proteins was also observed in wild-type mice treated with clofibrate, a potent PPARα activator; however, the degree of the induction of AOX and PT in the transgenic mice was smaller than that in the clofibrate-treated wild-type mice (Fig. 3), suggesting that the PPARα activation found in the transgenic mice was not as intense as that in the mice treated with clofibrate.

Histological evaluation of PPARα activation

An increase in the numbers of peroxisomes is associated with PPARα activation.[18] To determine whether peroxisome proliferation occurs in the HCV core gene transgenic mice, cytochemical staining for peroxisomal catalase was performed. A scattered distribution of hepatocytes with numerous peroxisomes was observed in the 9-month-old transgenic mice (Fig. 4*a*). Such hepatocytes were also found in the 22-month-old transgenic mouse livers (Fig. 4*a*). In contrast, almost all of the hepatocytes in the clofibrate-treated mice showed significant peroxisome proliferation (Fig. 4*a*). To quantitatively evaluate the degree of peroxisome proliferation, morphometric analysis of peroxisomes was conducted. The numerical density and volume density were significantly increased in the transgenic mice compared with those in the nontransgenic mice (Fig. 4*b*). The volume density, the most reliable parameter of peroxisome proliferation, was increased age-dependently in the transgenic mice, but the degree of the increase was not as prominent as that observed in mice with clofibrate administration (Fig. 4*b*). The finding that only some hepatocytes in the transgenic mice presented a marked peroxisome proliferation (Fig. 4*a*) is noteworthy, since it seems to correlate with the finding that intense expression of the core protein was observed only in particular hepatocytes.[10] These histological analyses reveal that spontaneous, continuous and age-dependent peroxisome proliferation and PPARα activation occur heterogeneously in the transgenic mouse livers, which is different from the response observed in the mice receiving clofibrate treatment.

Appearance of PPARα-, and cyclin D1-positive hepatocytes

We tried to detect abnormal hepatocytes to clarify the mechanism of hepatocarcinogenesis in the transgenic mice. On PPARα immunofluorescence staining, PPARα was primarily detected in the cytoplasm of the nontransgenic mice and the clofibrate-administered mice. Some hepatocytes having nuclei positively stained